TEXAS A&M UNIVERSITY
College Station, Texas

TEXAS TRANSPORTATION INSTITUTE

ASPHALT OVERLAYS WITH MIRAFI® FABRIC - THE SLIPPAGE QUESTION - ON AIRPORT PAVEMENTS

by

Jon A. Epps
Research Engineer

and

Joe W. Button
Assistant Research Engineer

Interim Report RF 3424-2

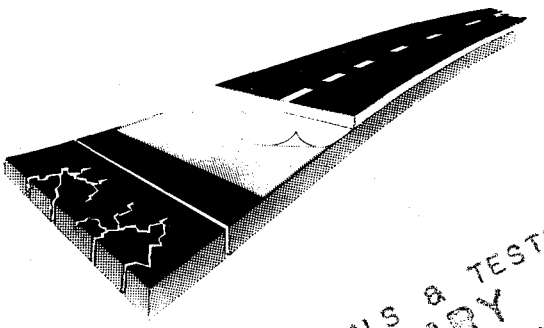

September-77

EXECUTIVE SUMMARY

Several factors work together to resist slippage in a layered asphaltic pavement system: mechanical interlock; interfacial adhesion; and tensile, compressive, and shear strength of the uppermost layer. Nevertheless, slippage has been observed on several commerical airfields and even on a few highways, particularly in areas of high shear stress. Generally, the crack is formed by the horizontal displacement of an asphalt concrete surface relative to the adjacent underlying structural layer. A typical slippage crack is crescent shaped with the arched ends pointed in the direction opposite that of tire motion (Figure i). When a slippage crack of this configuration is observed in a pavement, all of the following have most likely occurred:

a. The shear stress produced by the braking tire was in excess of the shear strength of the interface.

b. The tensile strength of the overlay was exceeded, producing a crack behind the braking tire.

c. The shear strength of the overlay was exceeded, producing a crack along the side of the braking tire.

d. The compressive strength of the overlay was exceeded, producing a shoved area in front of the braking tire.

Increased interest in using fabric membranes in airport overlay applications has raised the question: How does a fabric affect the interfacial shear strength between the old pavement and new overlay? Since interfacial shear strength is one of four possible contributors to slippage, this report discusses this effect for one particular membrane - Mirafi® 140 fabric.

Mirafi® is a trademark of Fiber Industries, Inc., a subsidiary of Celanese Corporation.

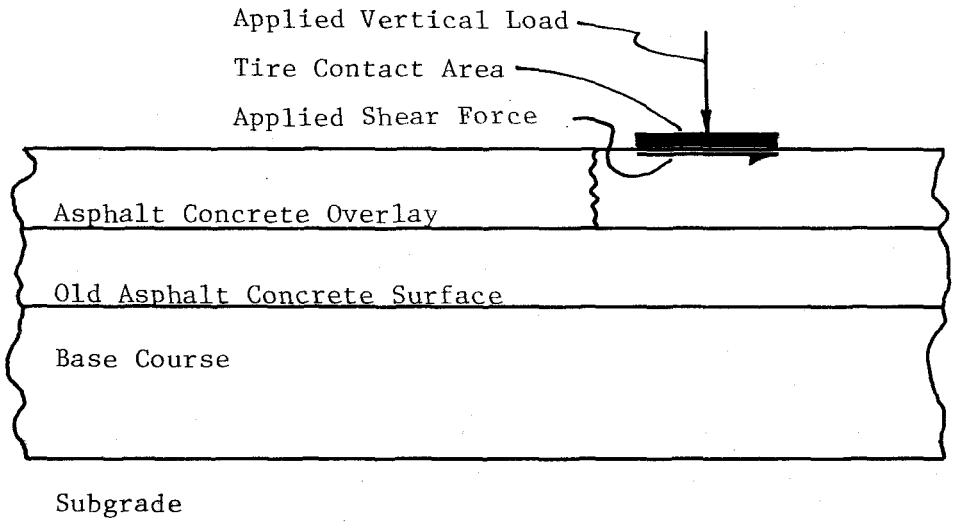

a. Side View

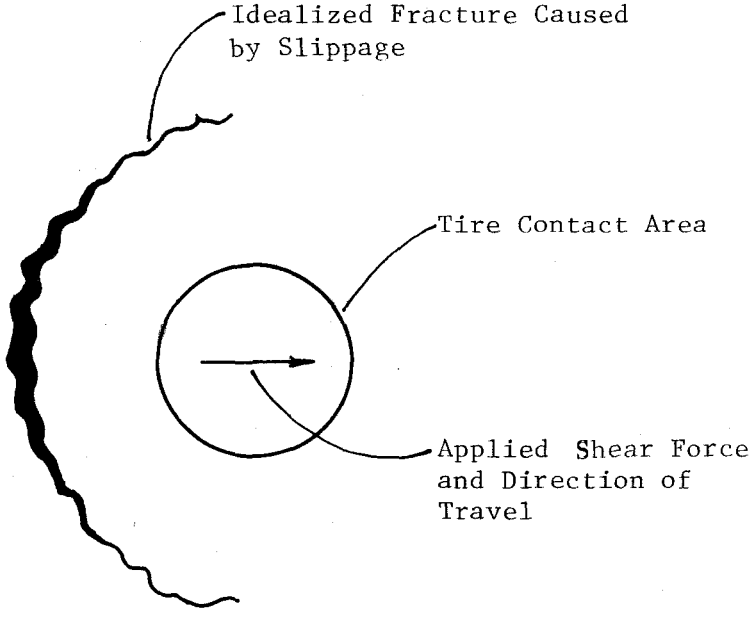

b. Top View

Figure i Typical Slippage Failure

Shear strength of layered asphalt specimens was measured in the laboratory. The test specimens were prepared by compacting two 1-inch layers of asphalt concrete, applying a layer of Mirafi 140 fabric, then compacting another 1-inch layer of asphalt concrete. Each specimen was tested for shear strength between layers at a deformation rate of approximately 13 inches per second (33 cm/sec) while applying a static vertical unit stress of 67 psi (460 kPa). Failures were produced in approximately 0.022 seconds.

The influence of tack coat quantity on shear strength for the overlay with and without Mirafi fabric is shown in Figure ii. A slight increase in shear strength was evident when the tack coat was increased on the non-fabric overlay from 0.05 to 0.10 gallon per square yard. The shear strength of overlays with fabric was apparently not very sensitive to tack coat quantity within the range tested. Obviously, inadequate tack coat will not provide adhesion between layers, and conversely, excessive tack coat will destroy the mechanical component of the bond and slippage may occur within the tack coat, especially at high temperatures.

The effect of test temperatures on shear strength was much more pronounced than the effect of tack coat quantity. As expected, the shear strength decreased markedly with an increase in temperature (Figure iii). Shear strength of the test specimens with and without fabric was almost identical at 104°F (40°C) and 140°F (60°C); however, at 68°F (20°C) the test specimens without fabric exhibited an increase in shear strength of about 30 percent more than the specimens with fabric. The reason for this difference at the lower temperature is not readily apparent.

A computer simulation was used to demonstrate an important tool useful to the engineer in estimating shear stresses that a pavement may experience. From the output of this computer program, one would not normally expect

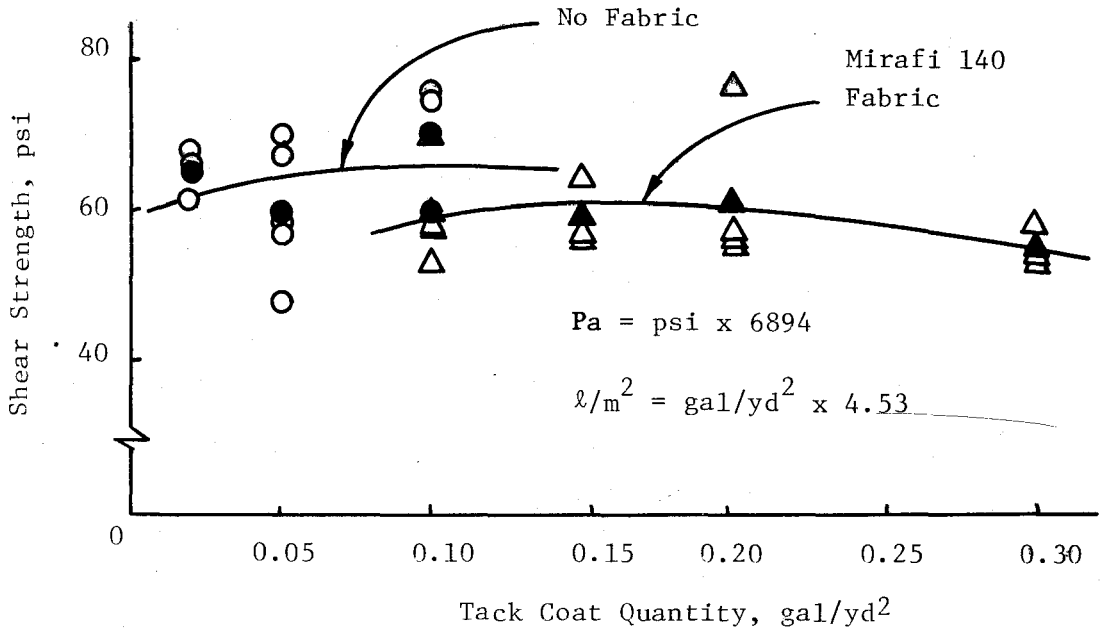

Figure ii Shear Strength as a Function of Tack Coat at 104°F (40°C)

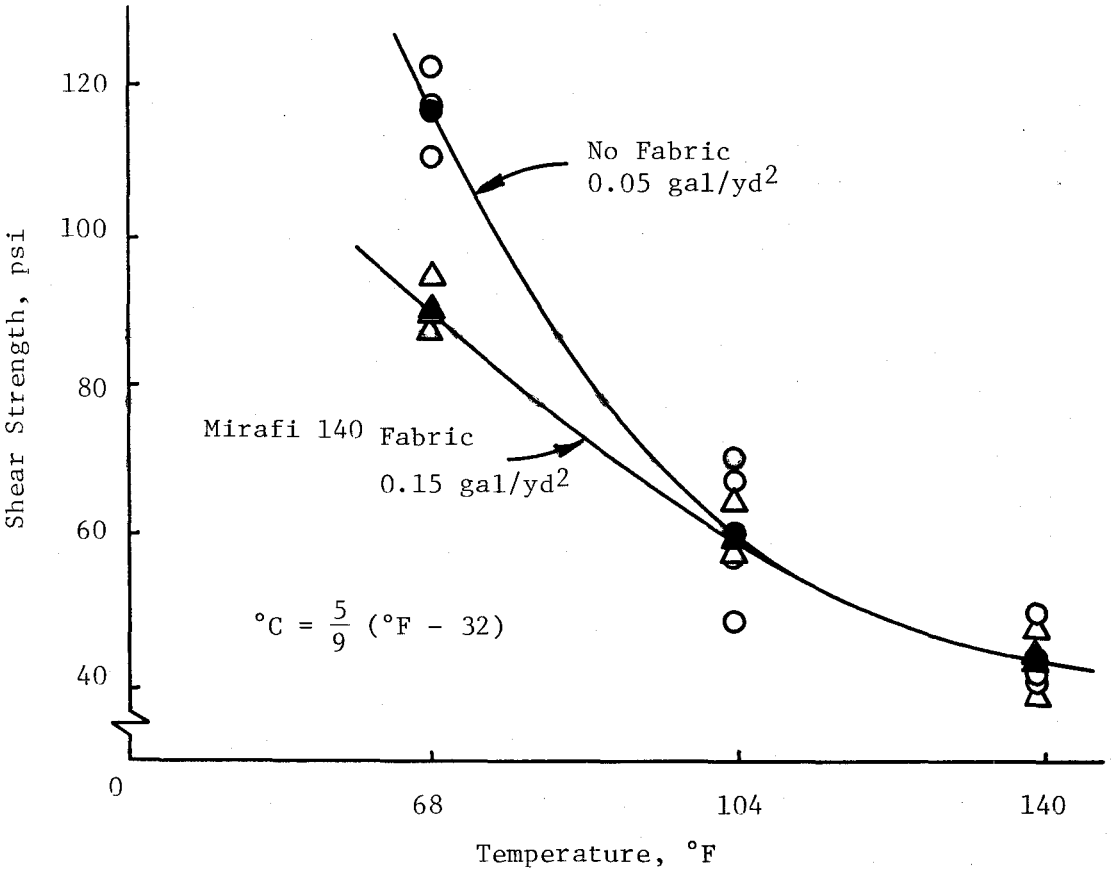

Figure iii Shear Strength as a Function of Temperature

slippage when a Beech King-Air applies brakes on a given overlaid pavement, but one would expect slippage when a Boeing 727 lands on the same pavement. Field experience, on the other hand, has indicated that slippage will occur only occasionally when a Boeing 727 lands. This indicates that interfacial shear strength between the layers is not the only factor that prevents slippage, but that tensile, compressive, and shear strength of the overlay also contribute in this regard.

Based on the data and analyses within the scope of this research, the following conclusions are given:

1. Mirafi 140 fabric does not affect the interfacial shear strength of an asphalt overlay at higher temperatures where shear strength becomes critical.

2. Mirafi 140 fabric will decrease the interfacial shear strength of an asphalt overlay at lower temperatures where shear strength is already more than adequate.

3. Mirafi 140 fabric will not compound slippage problems when used in preventing reflection cracking on overlaid runways and highways.

TABLE OF CONTENTS

LIST OF FIGURES

LIST OF FIGURES (CONT'D)

LIST OF TABLES

INTRODUCTION

Slippage of asphalt concrete overlays has been observed on several commercial airfields in the last ten years. These failures have been associated with high-performance aircraft and are exhibited in the areas of aircraft braking and/or turning movements. Slippage has also been noted on highways; however, these failures are not widespread and they are usually located in the wheel path or in other areas of high shear stress.

Typically, slippage cracks are crescent shaped with the arched ends of the crack pattern pointed in the direction opposite that of vehicle travel (Figure 1). The crack is formed by the horizontal displacement of one layer of pavement relative to another. Generally, the asphalt concrete surface moves relative to the base course or an underlying pavement (1, 2). To prevent slippage it is therefore important that "sufficient" bond be obtained between the asphalt concrete surface or wearing course and its underlying materials. Thus, to prevent slippage the engineer can control two factors: 1) the strength of the interfacial bond between the pavement layers and 2) the magnitude of the shear stress applied by traffic.

A strong bond to resist slippage is achieved at the interface by both mechanical interlock and adhesion. Adequate interlock of rough textured surfaces composed of angular aggregates resists slippage. To improve adhesion a cutback asphalt prime coat is normally utilized between an untreated base course and the asphalt concrete, and an emulsified asphalt or asphalt cement tack coat is utilized between layers of asphalt concrete. The proper amount of tack coat is usually 0.05 to 0.10 gallon of asphalt cement per square yard. Inadequate tack coat will not provide adhesion

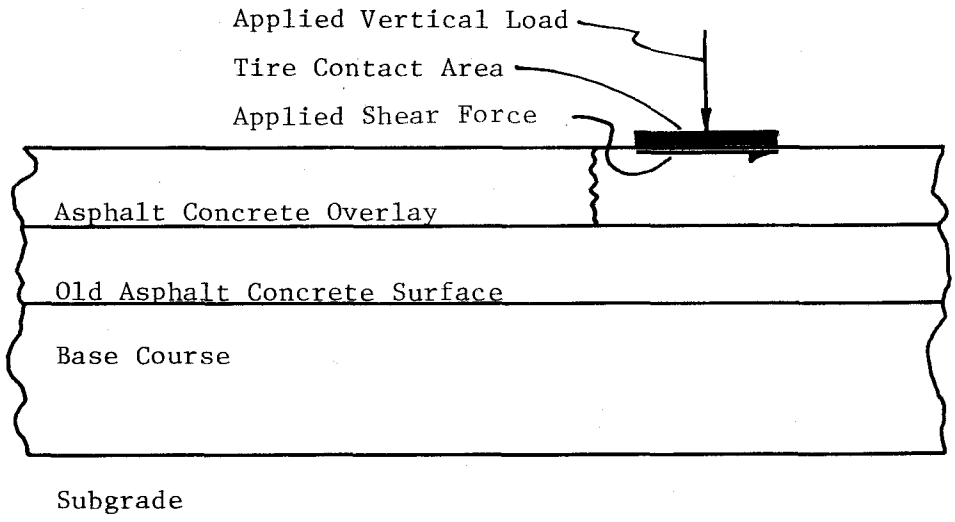

a. Side View

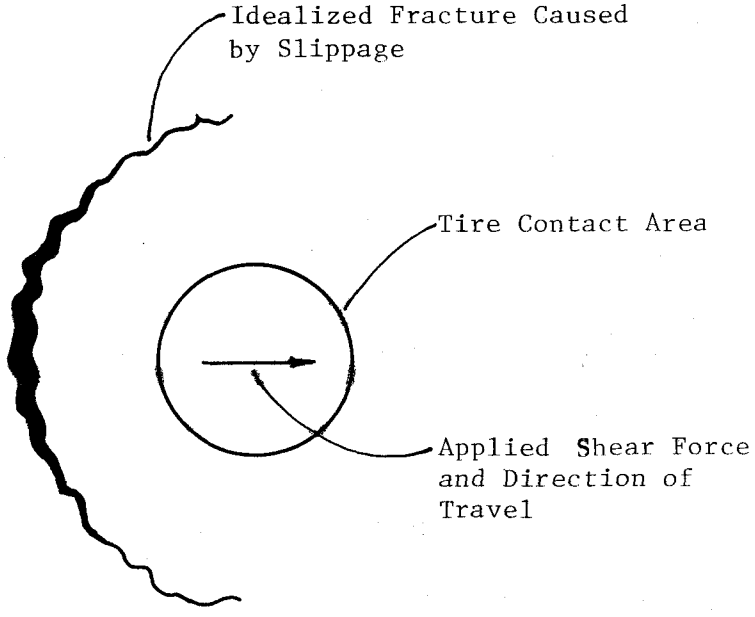

b. Top View

FIGURE 1. Typical Slippage Failure

between the layers. Excessive tack coat will destroy the mechanical component of the bond and slippage may occur in the tack coat itself, particularly at high temperatures.

The control of the shear stress imposed on the interface between the pavement layers is primarily achieved by selection of the thickness of the asphalt concrete surface course. The engineer normally designs the pavement structure for the imposed traffic including axle load, load repetitions and tire pressure.

Fabrics like Mirafi 140 have been utilized between old asphalt concrete pavements and new asphalt concrete overlays to reduce reflection cracking. As a result of these trials, a number of questions have been raised; included among these are: 1) What is the potential for slippage for this type of construction? 2) What can the design engineer do to reduce the likelihood of slippage if a fabric is to be utilized? Information is presented in this report in an attempt to answer these questions. Specifically, the results of a limited laboratory test program are presented together with the results of calculations which describe the magnitude of the shear stress at the interface between an overlay and the existing substrate.

LABORATORY STUDY

General

Laboratory testing equipment was developed and used to test the interfacial shear strength of asphalt concrete mixtures at a rapid rate of loading, with a positive vertical pressure and at temperatures representative of those found in pavements. The test conditions were selected to duplicate as nearly as possible the conditions which produce slippage in the field on airport runways.

Specially prepared asphalt test specimens were subjected to shear tests at three temperatures: 68, 104, 140°F (20, 40, 60°C). The specimens were fabricated as follows: 1) an overlay with Mirafi 140 fabric, 2) an overlay without fabric, and 3) control (containing no pavement-overlay interface). Different quantities of tack coat were applied to those specimens fabricated with and without fabric.

Materials

The asphalt cement and aggregate utilized in the fabrication of asphalt concrete test specimens are currently used as laboratory standards in the Texas A&M University materials testing laboratory (3). Tables and figures describing these materials in detail are in Appendix A.

Asphalt. The asphalt material selected for use in this study is a viscosity-graded AC-10 petroleum asphalt cement produced by the American Petrofina Company. Standardized tests (4, 5, 6) were performed on the original asphalt to determine the basic physical and chemical characteristics. The results of these tests are summarized in Table A1 of Appendix A.

Aggregate. A very hard crushed limestone was obtained from White's Mines at a quarry near Brownwood, Texas. This material has been selected

as one of two standard aggregates and as such is stored separately sized from 3/4-inch to minus No. 200 mesh. Samples of the various sized fractions are shown in Figure A1. Prior to mixing with asphalt, the various aggregate sizes were recombined according to the ASTM D3515-77 5A grading specification. The project gradation design as well as the upper and lower limits of the specifications are shown in Figure A2. Standard tests (4, 5, 6) were conducted to determine various physical properties of the aggregate. The types of tests and results are presented in Table A2.

Mixture. Mixtures of these materials containing various quantities of asphalt cement were tested using the Marshall Method (4) and the Hveem Method (7) to determine the optimum asphalt content. The optimum asphalt content is 4.5 percent by weight of aggregate.

Resilient modulus (a measure of stiffness) of the mixtures was determined at 68°F (20°C) using the Mark III Resilient Modulus Device developed by Schmidt (8).

The splitting tensile test was conducted at 68°F (20°C) with a loading rate of 2 inches per minute. Stress, strain, and modulus of elasticity were computed at the point of failure using a value of 0.35 for Poisson's Ratio (9).

A summary of the test results is given in Table A3, where each value represents an average of three test specimens.

Fabric. The fabric, Mirafi 140, was supplied by Celanese Fibers Marketing Company. Mirafi 140 fabric is a unique nonwoven fabric constructed from two types of continuous-filament fibers. One is a polypropylene homofilament, and the other is a heterofilament comprised of a polypropylene core covered with a nylon sheath. A random mixture of these filaments is formed into a sheet that is heat-bonded; the result is direct fusion at points

of contact between heterofilaments. No bonding agent or resin is used. The polypropylene filaments remain unaffected during the heat-bonding process. Purely mechanical links operate between these homofilaments (10).

Fabrication of Test Specimens

The materials described above were used to fabricate 3 x 3 x 15-inch (7.6 x 7.6 x 38 cm) asphalt concrete beams at the optimum asphalt content. The beams were compacted in three 1-inch (2.5 cm) layers at 250°F (121°C) by applying 28 tamps to the first two layers and 56 tamps to the third layer using a 2-inch by 3-inch tamping foot at 225 psi (1.55×10^6 Pa) contact pressure. Six control specimens were prepared by sawing across the length of the beam to produce 3 x 3 x 2-inch (7.6 x 7.6 x 5.1-cm) blocks. Several more of these beams were selected and the following procedures were used in the preparation of the remaining test specimens:

1. Saw away the top 1 inch to produce 2 x 3 x 15-inch (5.1 x 7.6 x 38-cm) beams.

2. Artificially weather the face opposite the sawn face by scrubbing with detergent and water using a brass-bristle brush.

3. Allow specimen to thoroughly dry.

4. Apply asphalt tack coat (AC-10) to the weathered face in quantities ranging from 0.02 to 0.30 gallon per square yard (0.113 to 1.36 ℓ/m^2).

5. If applicable, apply Mirafi 140 fabric (lot 68606) to tack coat and smooth with gloved fingertips.

6. Replace specimen in mold and compact a 1-inch layer of asphalt concrete over the fabric to produce 3 x 3 x 15-inch specimens.

7. Saw across the length of the specimen to produce 3 x 3 x 2-inch (7.6 x 7.6 x 5.1-cm) blocks and label each.

Testing of Specimens

The specimens were divided into three groups and placed in environmental rooms controlled separately at 68, 104, 140°F (20, 40, 60°C). After a time sufficient for the specimens to reach the appropriate temperature, a few at a time were placed in a box and surrounded with expanded polystyrene chips, then conveyed to the test laboratory. Each specimen was placed in the shear tester (Figure 2) and immediately tested to insure no appreciable temperature change. The shear tests were conducted at a deformation rate of approximately 13 inches per second (33 cm/sec) while applying a static vertical load of 400 pounds (182 kg) or a unit pressure of 67 psi (4.6×10^5 Pa). Failures were produced in about 0.022 second with this lateral translation rate.

Laboratory Test Results

A summary of the test results is presented in Tables 1 and 2 and Figures 3 through 6.

The control specimens, which had no layer interface along the shear plane, had an average shear strength of 70 psi at 104°F (40°C). This strength was only slightly higher than that measured for the overlaid test specimens tested at the same temperature (Table 1 and Table 2).

The influence of tack coat quantity on shear strength for overlaid specimens with and without fabric is shown in Figure 3. A slight increase in shear strength was evident when the tack coat was increased on the non-fabric overlay from 0.05 to 0.10 gallon per square yard. The shear strength of overlays with fabric was apparently not very sensitive to the tack coat quantity. Investigation of shear strength of fabric overlays at tack coats below 0.10 and above 0.30 gallon per square yard would in all probability show a decrease (Figure 3), as tack coat quantities of about 0.10 gallon per square

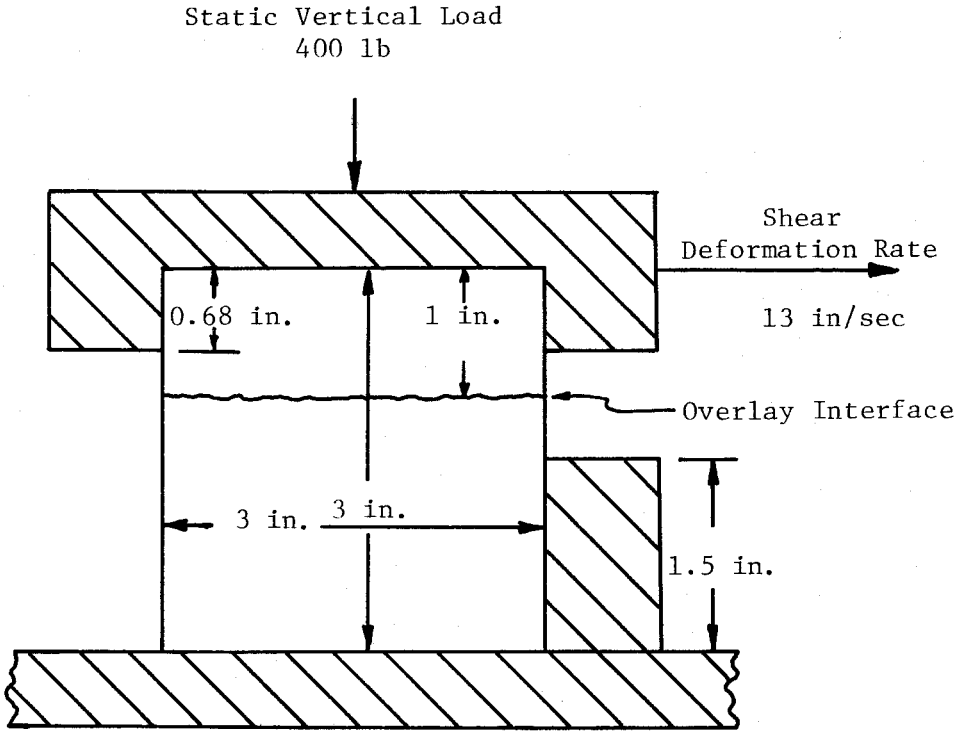

FIGURE 2. Schematic of Shear Test Apparatus

Table 1. Test Results of Samples Containing No Fabric

Sample No.	Tack Coat, gal/yd^2 (ℓ/m^2)	Test Temp. °F (°C)	Shear Stress @ Failure, psi (Pa x 10^5)	Mean Shear Stress @ Failure, psi (Pa x 10^5)	Standard Deviation
C-1	0.0 Control Samples	104 (40)	72 (4.96)	70 (4.83)	4.2
C-2			72 (4.96)		
C-3			64 (4.41)		
C-4			70 (4.83)		
C-5			67 (4.62)		
C-6			76 (5.24)		
C-7	0.02 (0.09)	104 (40)	66 (4.55)	65 (4.48)	3.6
C-8			68 (4.69)		
C-9			61 (4.21)		
C-10	0.05 (0.23)	68 (20)	120 (8.27)	116 (8.00)	5.1
C-11			117 (8.07)		
C-12			110 (7.58)		
C-13	0.05 (0.23)	104 (40)	70 (4.83)	63 (4.34)	5.7
C-14			67 (4.62)		
C-15			61 (4.21)		
C-16			57 (3.93)		
C-17			58 (4.0)		
C-18	0.05 (0.23)	140 (60)	41 (2.83)	43 (2.96)	4.9
C-19			49 (3.38)		
C-20			40 (2.76)		
C-21	0.10 (0.45)	104 (40)	76 (5.24)	70 (4.83)	8.7
C-22			60 (4.14)		
C-23			74 (5.10)		

Table 2. Test Results of Samples Containing Mirafi 140 Fabric

Sample No.	Tack Coat, gal/yd^2 (ℓ/m^2)	Test Temp. °F (°C)	Shear Stress @ Failure, psi (Pa x 10^5)	Mean Shear Stress @ Failure, psi (Pa x 10^5)	Std. Dev.	Fabric Remaining on Orig. Pavement, Percent
C-24	0.10 (0.45)	104 (40)	70 (4.83)	60 (4.14)	5.6	80
C-25			58 (4.00)			100
C-26			59 (4.07)			85
C-27			58 (4.00)			80
C-28			53 (3.65)			80
C-29			60 (4.14)			80
C-30	0.15 (0.68)	68 (20)	87 (6.00)	90 (6.20)	3.6	95
C-31			94 (6.48)			95
C-32			89 (6.14)			95
C-33	0.15 (0.68)	104 (40)	57 (3.93)	59 (4.07)	4.0	85
C-34			64 (4.41)			80
C-35			57 (3.93)			70
C-36	0.15 (0.68)	140 (60)	38 (2.62)	40 (2.76)	3.5	0
C-37			44 (3.03)			0
C-38			38 (2.62)			0
C-39	0.20 (0.91)	104 (40)	56 (3.86)	57 (3.93)	1.9	90
C-40			60 (4.14)			90
C-41			55 (3.79)			90
C-42			56 (3.86)			90
C-43			57 (3.93)			60
C-44	0.30 (1.36)	104 (40)	53 (3.65)	55 (3.79)	2.6	80
C-45			58 (4.00)			20
C-46			54 (3.72)			50

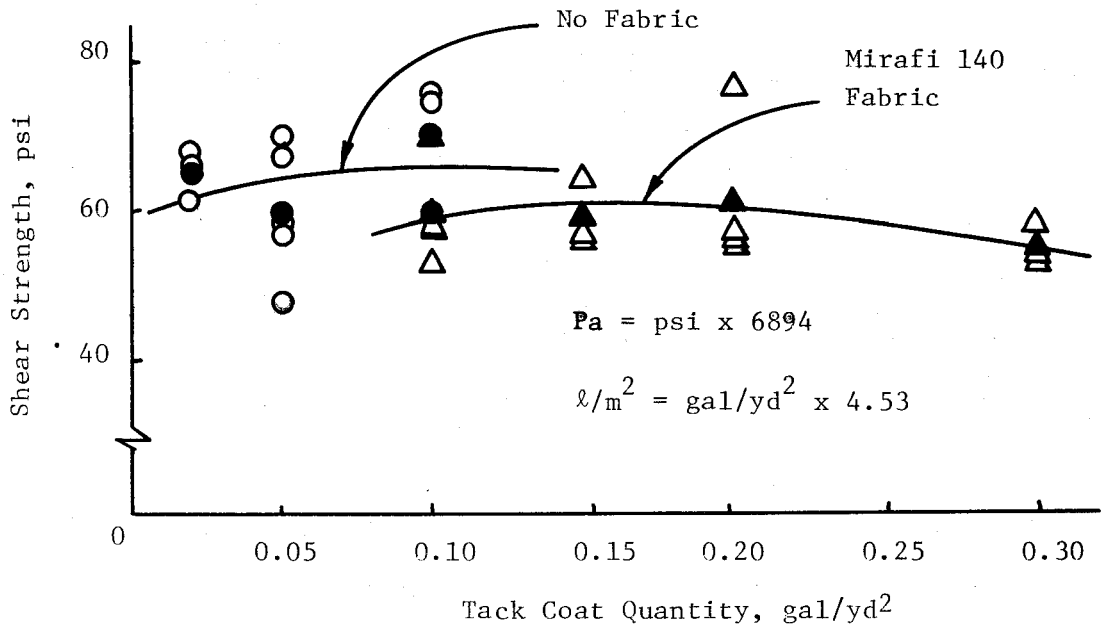

FIGURE 3. Shear Strength as a Function of Tack Coat at 104°F (40°C)

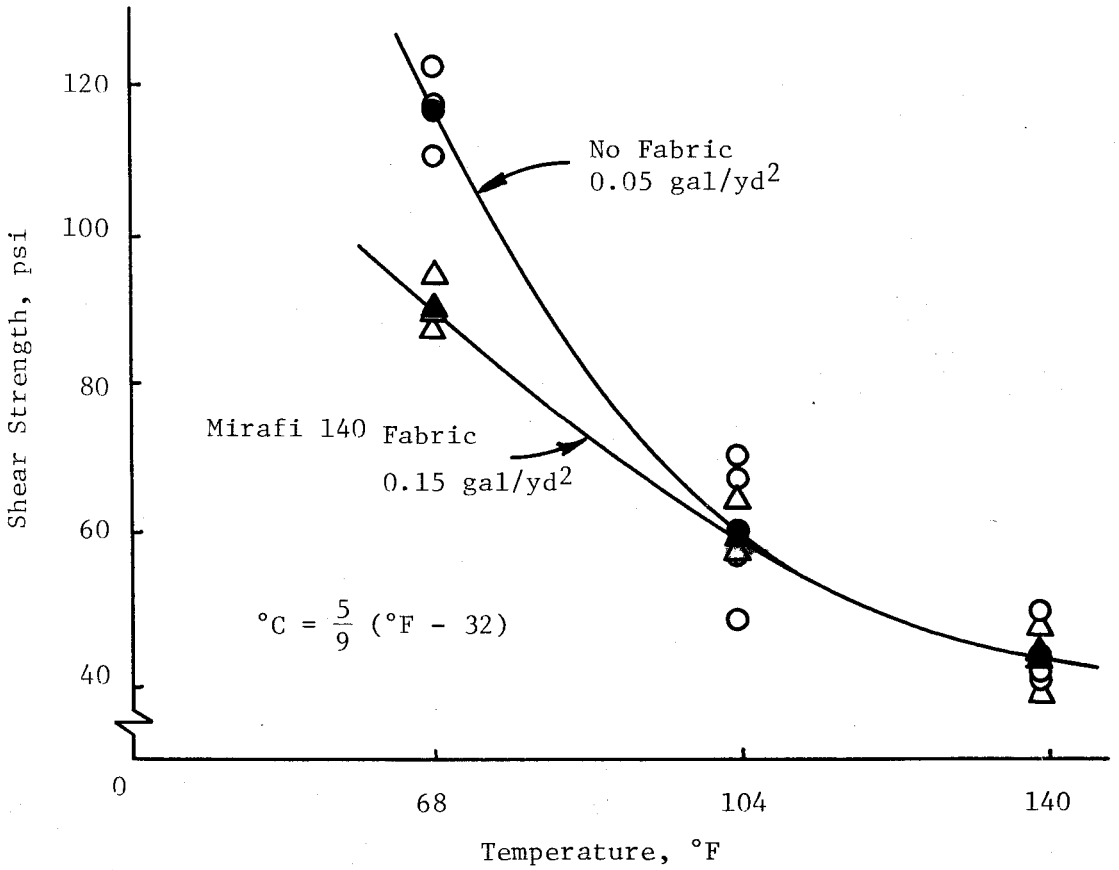

FIGURE 4. Shear Strength as a Function of Temperature

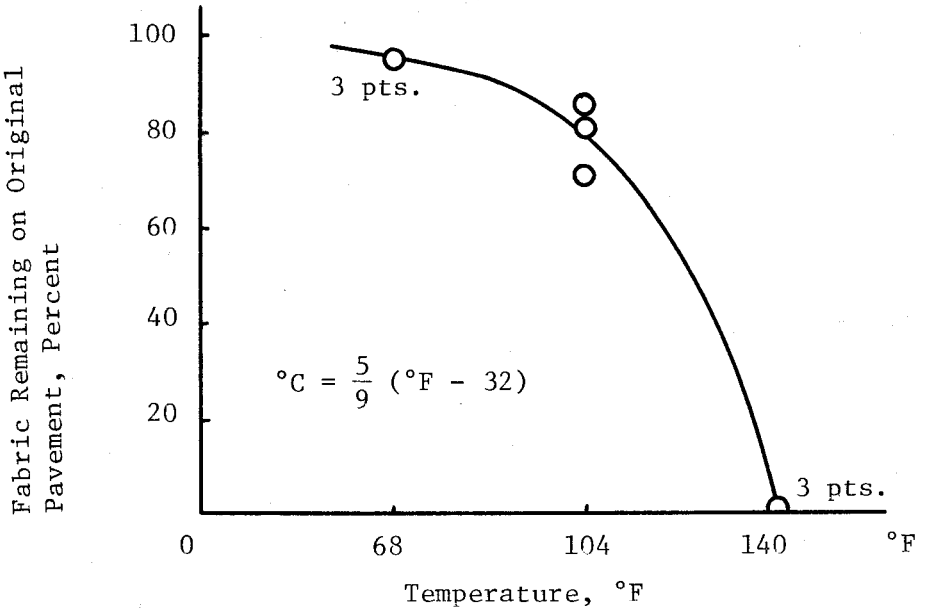

FIGURE 5. Mirafi 140 Fabric Remaining on Original Pavement after Shear Test with 0.15 gal/yd^2

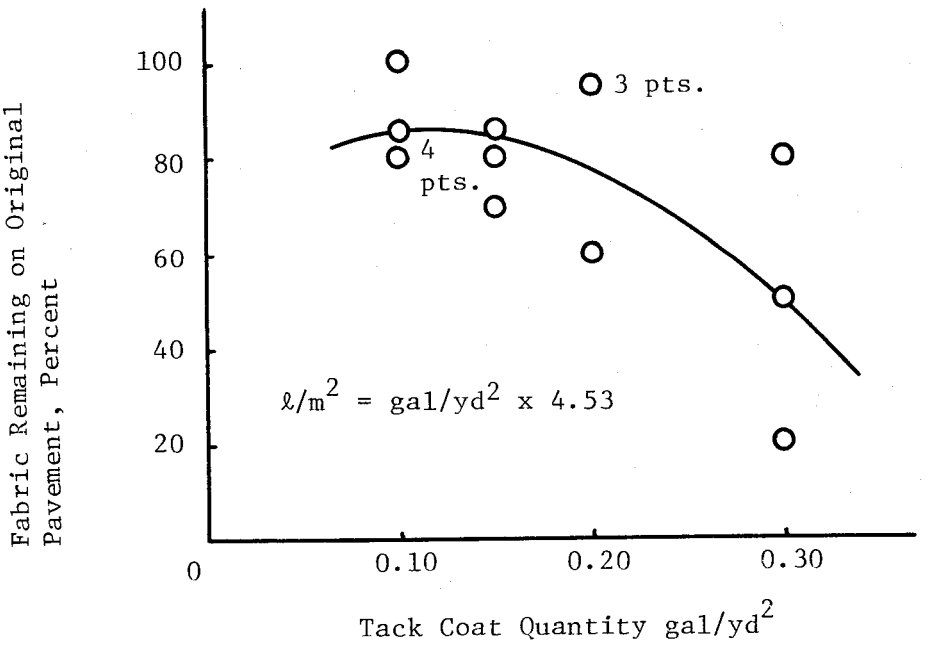

FIGURE 6. Mirafi 140 Fabric Remaining on Original Pavement after Shear Test @ 104°F (40°C)

yard are required for fabric saturation (11) and quantities in excess of 0.30 gallon per square yard would be expected to reduce the mechanical interlock between the old and new surface.

The effect of test temperatures on shear strength was much more pronounced than the effect of tack coat quantity. As expected, the shear strength decreased markedly with an increase in temperature (Figure 4). Shear strength of the test specimens with and without fabric were almost identical at 104°F (40°C) and 140°F (60°C); however, at 68°F (20°C) the test specimens without fabric exhibited an increase in shear strength of about 30 percent more than the specimens with fabric. The reason for this difference at the lower temperature is not readily apparent.

It is interesting to note the relationship between temperature and the approximate percentage of fabric remaining on the original simulated pavement after a shear test with 0.15 gallon per square yard of tack coat (Figure 5). By observation of the test specimens, it was determined that the shear failure zone at 68°F was located at the fabric/new-overlay interface. At 104°F, the failure zone for individual specimens occurred both at the fabric/old-pavement interface and at the fabric/new-overlay interface. At 140°F, failure occurred at both fabric interfaces and the fabric tended to fold or roll during testing. At high temperatures (as well as high tack coat quantities), it was difficult to determine whether the fabric rolled up or fabric failure occurred.

The relationship between tack coat quantity and the approximate percentage of fabric remaining on the original simulated pavement after shear testing is shown in Figure 6. At low tack coat quantities, the failure zone was located at the fabric/new-overlay interface; whereas, at high tack

coat quantities, the failure zone was located at both fabric interfaces. An increase in tack coat quantity appeared to produce results similar to an increase in temperature. From observation of the test specimens, it is surmised that this trend is due to the absorptive capacity of the fabric and/or the rheology of the asphalt cement. At low tack quantities and low temperatures, the tack material did not migrate to the upper surface of the fabric to sufficiently bind it to the overlay. At high tack quantities and high temperatures, migration took place and an excess of tack material was present at both fabric interfaces, which diminished the mechanical bond.

Discussion of Laboratory Test Results

Due to the limited nature of this investigation, a brief literature search was conducted to provide confidence in the reported shear strength of the asphalt concrete and the overlay interface. Results of this literature search have indicated shear strengths of asphalt concrete and shear strength of overlay interfaces have not been measured at high rates of loading of deformation. However, estimated tensile strengths of asphalt concrete mixtures can be obtained by use of nomographs developed by Heukelom (12) and a general relationship between shear strength and tensile strength (13) can be used to predict measured shear strength.

Tensile strengths for the asphalt concrete mixtures were predicted from Heukelom's nomographs (12) by employing the recovered asphalt cement properties, mixture composition characteristics, test temperature, and duration of loading. Predicted tensile strength at 104°F (40°C) for this mixture was 140 psi (9.7×10^5 Pa). Troxell, et al. (13) suggest that shear strength for portland cement concrete is approximately 20 to 30 percent greater than its tensile strength. Since the asphalt concrete specimens were tested at a relatively

high deformation rate, we may then realistically assume that they behaved elastically and hence apply this conversion. In doing so, a predicted shear strength of approximately 175 psi (1.2×10^6 Pa) was obtained compared to a measured shear strength of 70 psi (4.8×10^5 Pa). Based on the inherent variability of the nomograph solution, this difference is not surprising.

The results of varying the tack coat quantity in concert with varying temperature in the shear tests suggest the use of minimum acceptable quantities of relatively hard asphalt cements for tacking Mirafi 140 fabric in very hot climates, and conversely, in cold climates increased quantities of a softer asphalt cement should be used.

The important relationship obtained from the laboratory study was the observed similarity of the magnitude of the shear strength of the overlay systems with and without fabric at temperatures above 100°F. Since the high temperature strengths are normally critical, it is reasonable to conclude that the use of Mirafi 140 in overlay systems would not contribute significantly to slippage distress.

SHEAR STRESSES IN PAVEMENTS

The laboratory testing program defined the magnitude of the shear strength of pavement overlay interfaces for certain temperatures and a selected rate of deformation. To predict the probable occurrence of slippage, this measured shear strength must be compared with shear stresses in pavements caused by wheel loads. The principal sources of pavement shear stresses are the vertical load on a tire (weight of vehicle), the applied horizontal load (braking force), and the weight of the pavement materials (Figure 1). The stresses due to the weight of the pavement materials are normally relatively small and will not be considered further.

Vertical Loads

For vertical loads, the magnitude of the shear stress is controlled primarily by the tire pressure, the thickness of the surface layer and the ratio of the stiffness of the surface course to the stiffness of the base course (K_1). The thickness of the base course and the ratio of the stiffness of the base course to the stiffness of the subgrade (K_2) have only a minor effect on the magnitude of the shear stress. For example, a twofold increase in thickness of the base course will reduce the shear stress at the surface-to-base interface only about three percent (14).

The magnitude of the horizontal shear stress ratio at the pavement interface between the first layer and the second layer is shown in Figure 7 (14). The terms are defined as follows:

T_{rz} = horizontal shear stress,

P = vertical stress at pavement surface (tire pressure),

h_1 = depth of pavement layer No. 1,

h_2 = depth of pavement layer No. 2,

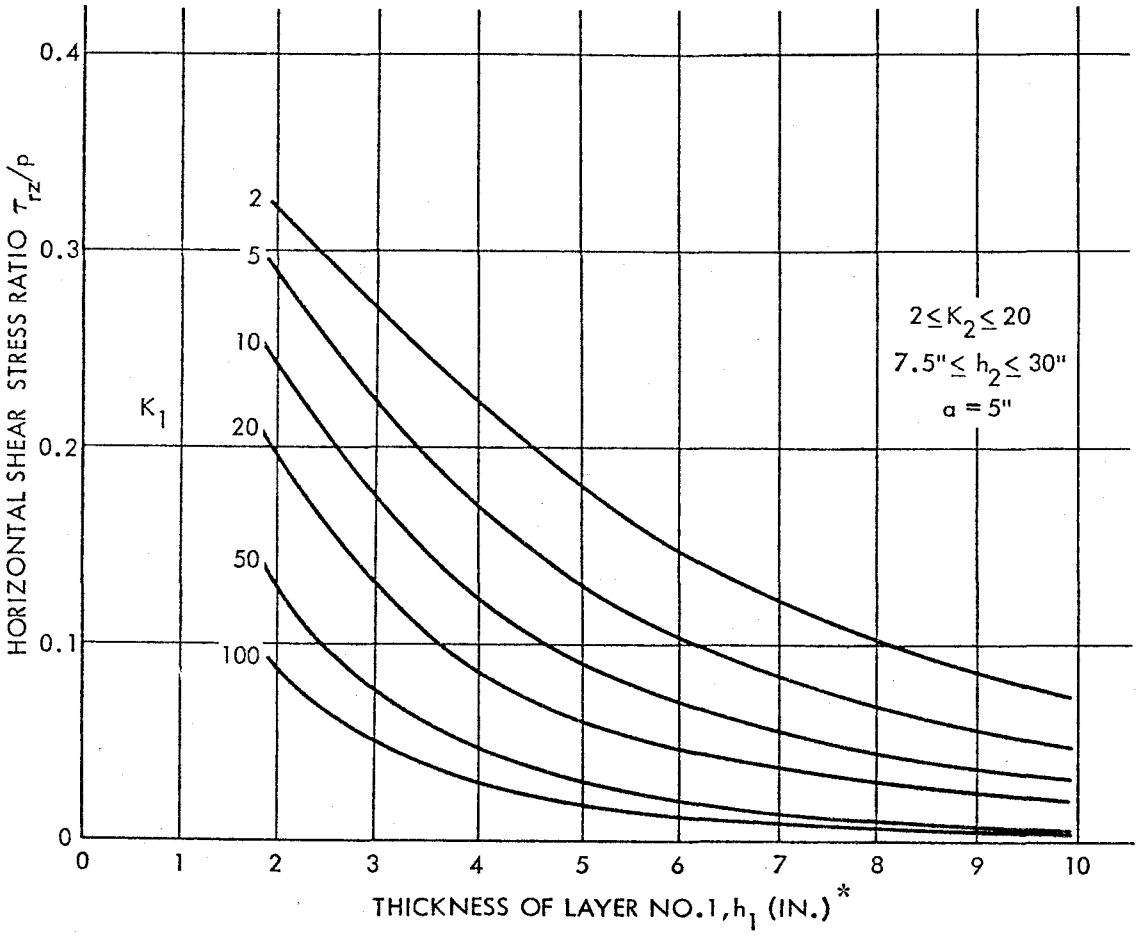

Figure 7. Variation in T_{rz}/p at the First Interface due to Vertical Load with K_1 and h_1

After reference (14)

*cm = 2.54 x in.

E_1, E_2 and E_3 = elastic moduli of layers 1, 2 and 3, respectively,

$K_1 = E_1/E_2$,

$K_2 = E_2/E_3$ and

a = radius of contact area (tire footprint).

As an example, let $h_1 = 2$ inches and $K_1 = 2$. From Figure 7, T_{rz}/p is found to be 0.32. A tractor-trailer truck has a tire footprint radius (a) of approximately five inches. Therefore, Figure 7 is valid for this vehicle. If the tire pressure (p) is 90 psi, then horizontal shear stress may be computed as follows:

$$T_{rz} = (T_{rz}/p) \times p = (.32)(90) = 29$$

Performing this operation for various values of h_1 produces a series of values for T_{rz} (Figure 8). If a similar operation is performed using tire pressure data from Table 3, then curves are generated on Figure 8 for the Beech King-Air and the Boeing 727. (However, since the tire footprint radius of the Boeing 727 is much larger than five inches, a small error is introduced.)

Thus from a design standpoint, the engineer can control the magnitude of the shear stresses at the overlay interface caused by vertical loads by use of the following techniques;

1) increase thickness of the overlay (increase h_1),
2) increase the ratio of the stiffness of the overlay material relative to the stiffness of the old pavement (increase K_1) and
3) reduce the tire pressure of the vehicles using the pavement (decrease p).

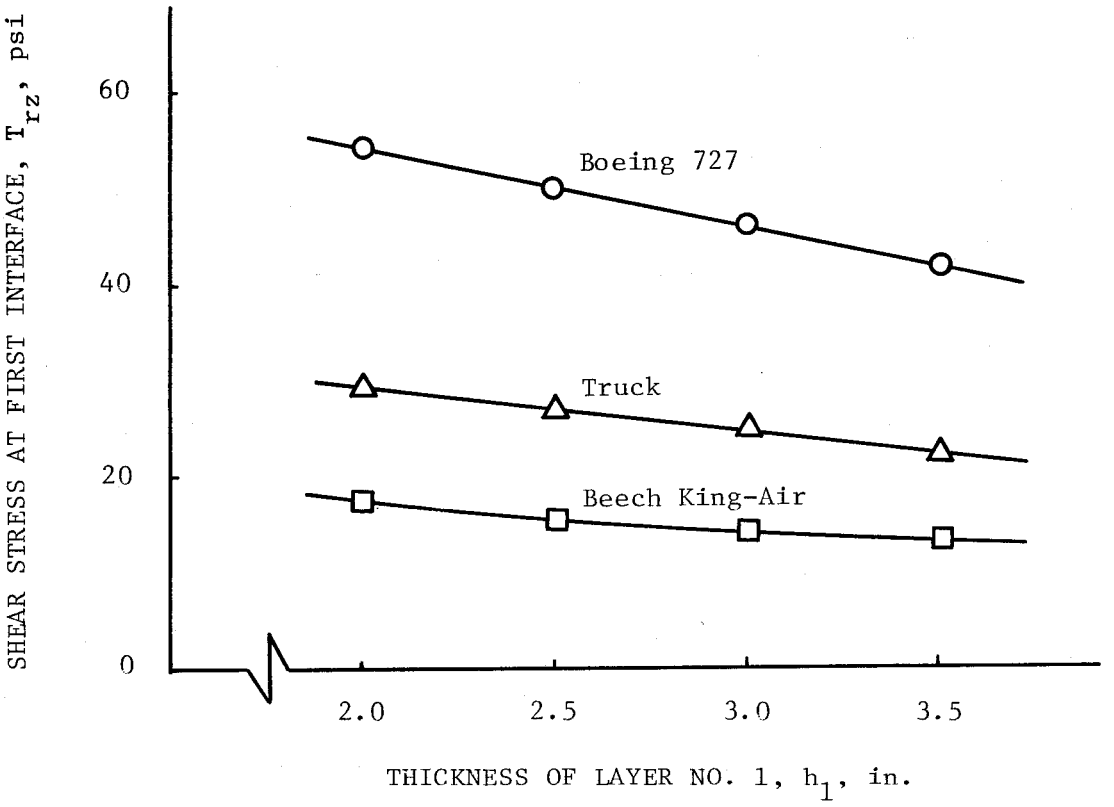

FIGURE 8. Variation in Shear Stress at the First Interface Due to Vertical Load

Horizontal Loads

Simplified relationships have not been developed for the determination of shear stresses due to applied braking forces for layered pavements. However, computer programs are available to aid the engineer in solving this complex problem.

Computer Simulation

The following paragraphs describe two computer programs that were used to estimate stresses in multi-layered pavements.

Description of Pavement. From subgrade to surface, the simulated, multi-layered pavement may be assumed to consist of the following layers: 1) a subgrade of infinite depth with an elastic modulus of 5,000 psi (3.4×10^4 kPa) and a Poisson's ratio of 0.35, 2) a 12-inch granular base with an elastic modulus of 50,000 psi (3.4×10^5 kPa) and a Poisson's ratio of 0.35, 3) a 3-inch (7.6 cm) asphalt concrete pavement with an elastic modulus of 800,000 psi (5.5×10^6 kPa) and a Poisson's ratio of 0.40 and 4) an asphalt concrete overlay of various depths including 2.0, 2.5, 3.0, 3.5 inches (5.1, 6.4, 7.6, 8.9 cm) also with an elastic modulus of 800,000 psi and a Poisson's ratio of 0.40.

Description of Aircrafts. The Boeing 727 Model 200 has a maximum ramp weight of 161,000 pounds (73,180 kg). This places it in a medium-size aircraft category.

The Beech King-Air is a small aircraft which has a maximum ramp weight of 9,300 pounds (4227 kg) and accommodates ten passengers. Tire and load data are given in Table 3.

TABLE 3. Aircraft Data for Computer Simulation

	Boeing 727	Beech King-Air
Maximum ramp weight, lb (kg)	161,000 (73.180)	9300 (4227)
Maximum weight per truck tire, lb (kg)	39,950 (18.160)	4700 (2136)
Truck tire footprint area, $in.^2$ (cm^2)	238 (1535)	90 (581)
Truck tire pressure, psi (kPa)	168 (1158)	52 (358)
Max. shear stress, psi (kPa) (Coef. friction = 0.8)	132 (910)	42 (290)
Assumed radius of tire footprint, in. (cm)	8.7 (22.1)	5.3 (13.5)

Description of Programs. Consider the instantaneous application of the brakes of an aircraft while traversing an overlaid runway pavement. Vertical as well as horizontal stresses are transmitted to the pavement to considerable depths.

Two computer programs, CRANLAY and UNCRANLAY (15), were used to predict stresses at various depths in multi-layered pavement systems due to vertical and horizontal load inputs at the surface. The program CRANLAY is used to compute the stresses, strains and displacements in a layered system under two axisymmetric circular loads: 1) uniform vertical pressure and 2) linear radial shear stress. Whereas, the program UNCRANLAY is used to compute corresponding stresses, strains and displacements in a layered system under one of two circular loads: 1) uniform unidirectional shear or 2) torsional shear. The material properties of each layer may be either isotropic, or cross-anisotropic with a vertical axis of symmetry. The interfaces between the layers are fully continuous. For values of pavement depth less than 0.2 times loaded radius (a), the numerical intergration procedure may not converge; however, this problem does not occur on the surface (15).

In this analysis, only vertical pressure and unidirectional horizontal shear in the pavement under a single tire were considered. The tire footprint was assumed to be circular and the loads uniformly applied over the circular area. The origin of the cylindrical coordinate system (R, θ, Z) is the center of the loaded circle. The stresses computed were under the center of the tire footprint in the vertical plane whose axis is in the same direction as that of the tire. Furthermore, these computed stresses were located ahead of (θ = 0°) and behind (θ = 180°) the center of the tire footprint at horizontal distances (R) of 0, 1/2R, R, 1.5R, 2R, and 3R and vertical distances (z) of 0, 1.75, 2.0, 2.5, 3.0, 3.5 and 4.0 inches

(0, 4.4, 5.1, 6.4, 7.6, 8.9 and 10.2 cm). The horizontal input load was estimated based on a coefficient of friction of 0.8 for the pavement surface. The resulting horizontal and vertical components of the pavement stresses computed by both CRANLAY and UNCRANLAY were algebraically summed using the appropriate sign convention. Stresses were computed for eight situations, which included two aircrafts on pavement overlays of four different depths. The results were tabulated and plotted and are presented in Appendix B.

Results from Computer Simulation

Longitudinal horizontal stresses in the overlaid pavements under the center of the tire were calculated and are presented in Appendix B. The stress distributions are shown in Figures B1 through B4 for the Boeing 727 and Figures B9 through B12 for the Beech King-Air. Stress distributions were plotted only at selected depths to reduce clutter on the graphs. These figures indicate the maximum shear stress occurs just ahead of the leading edge of the tire contact area where the stear stresses from both the horizontal and vertical loads act in the same direction. The horizontal shear stresses behind the center of the tire footprint generated by the vertical load oppose the shear stresses generated by the horizontal load. Theoretically, at the pavement surface, no horizontal stress is generated by the vertical load.

The corresponding vertical stress distributions in the overlaid pavements are shown in Figures B5 through B8 for the Boeing 727 and Figures B13 through B16 for the Beech King-Air. These stresses are due primarily to the vertical load, however, below the surface, small vertical stresses were generated by a moment caused by the horizontal load. Ahead of the tire center, these forces act downward, but behind the tire center they act upward. Evidence

of this, particularly at shallow depths, such as 1.75 inches, can be seen in the figures.

The maximum shear stress produced by a skidding vehicle is not always at the pavement surface (see Appendix B). Figures 9 and 10, prepared from data presented in Appendix B, illustrate that the depth of an overlay can govern the magnitude of the stresses experienced within a pavement. The magnitude of the shear stress within the pavement decreased with increased overlay depth to a depth of about 2.5 to 2.8 inches, then as depth increased further, the reverse trend became dominant.

The variation in shear stress at the first interface due to vertical plus horizontal loads is shown in Figure 11. For the Boeing 727 (heavier aircraft), the magnitude of the decrease in shear stress with increased overlay thickness is noticeably greater than that for the Beech King-Air. This indicates that increasing the thickness of an overlay applied for use by heavy traffic significantly reduces the magnitude of shear stress at the interface, whereas for light traffic, increased overlay thickness may accomplish relatively little regarding shear stress magnitude at the interface. However, on a percentage basis the reduction in shear stress with increase in surface thickness is comparable.

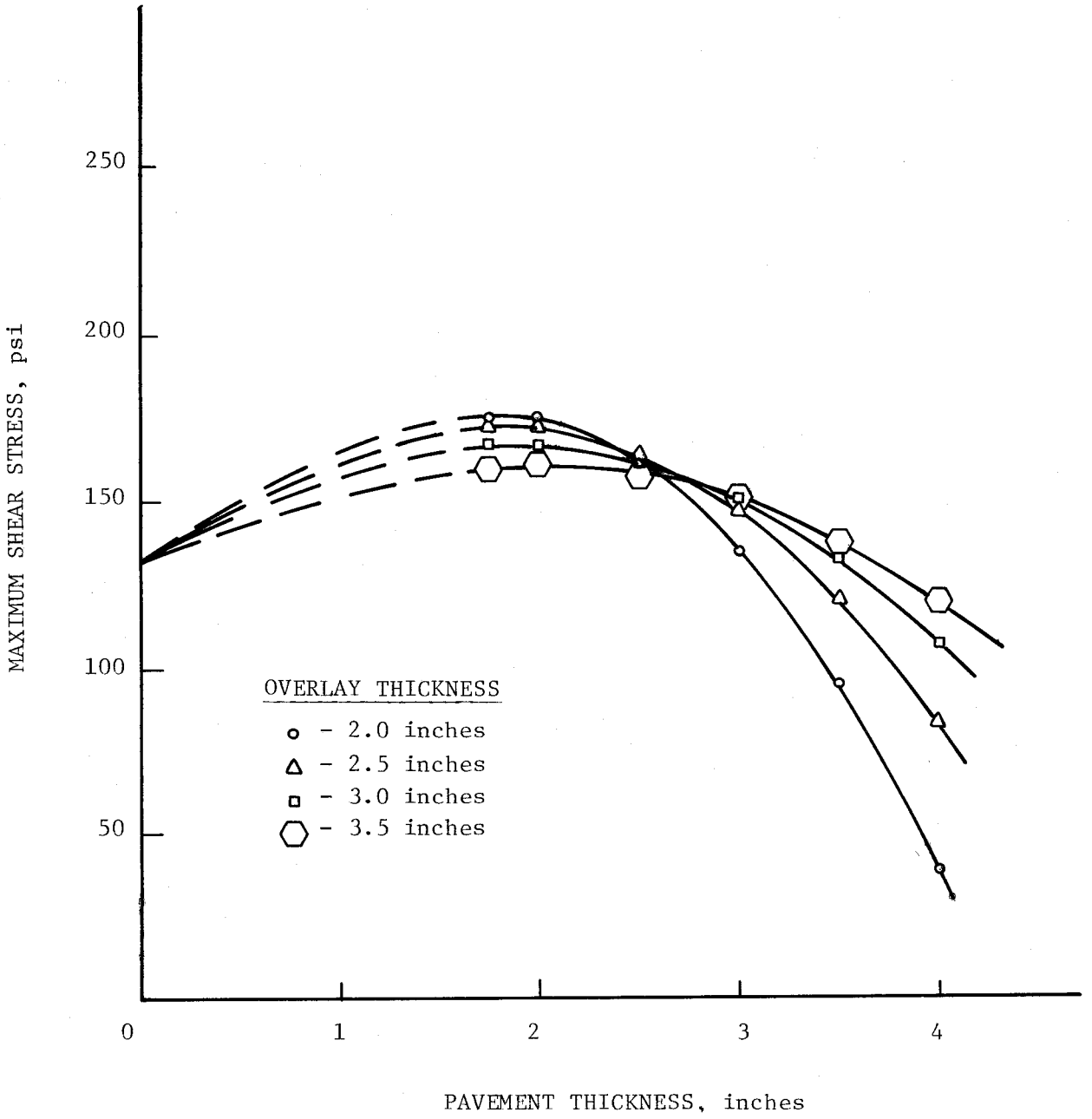

FIGURE 9. Maximum Shear Stress vs. Pavement Thickness for Boeing 727

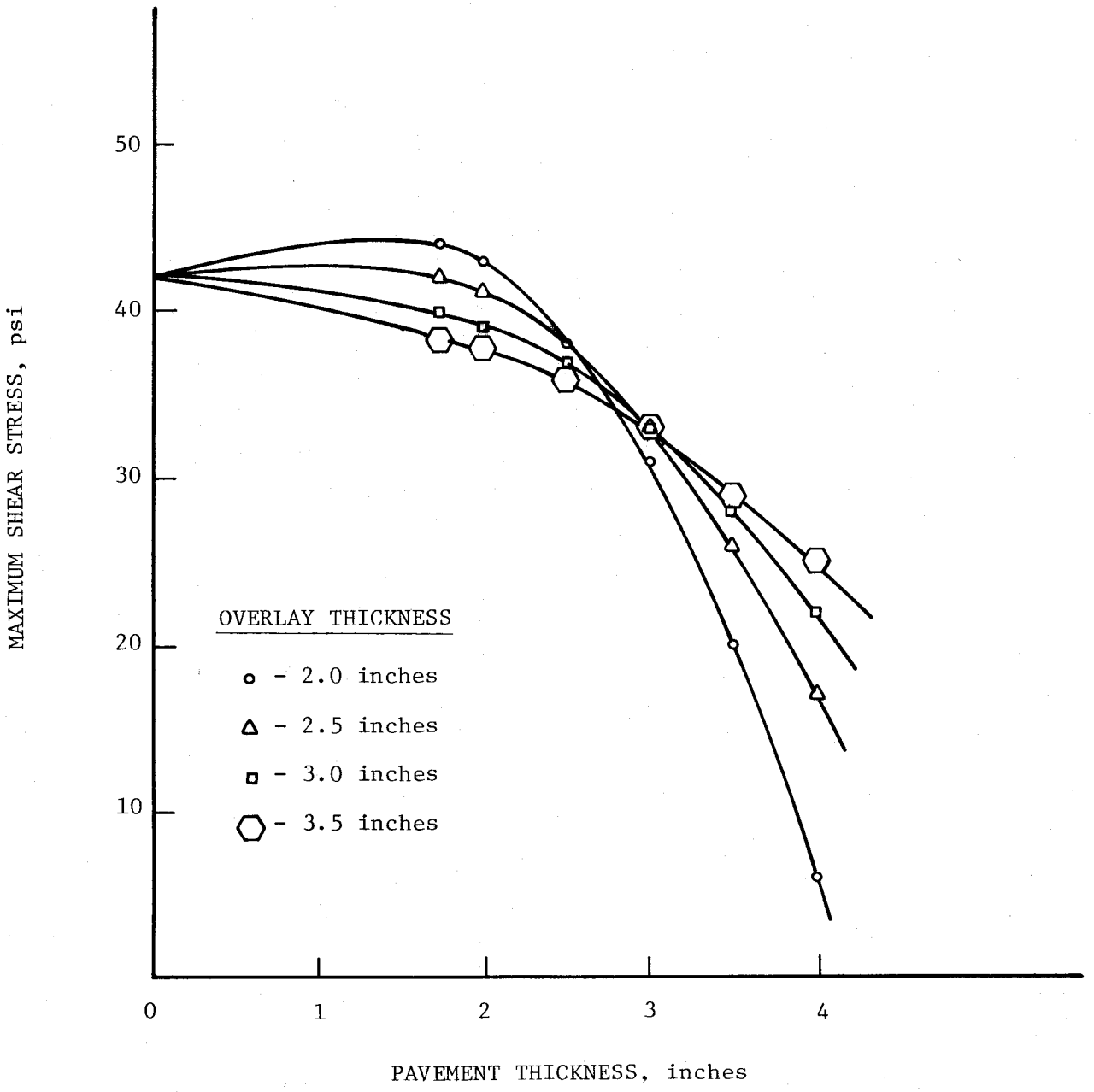

FIGURE 10. Maximum Shear Stress vs. Pavement Thickness for Beech King-Air

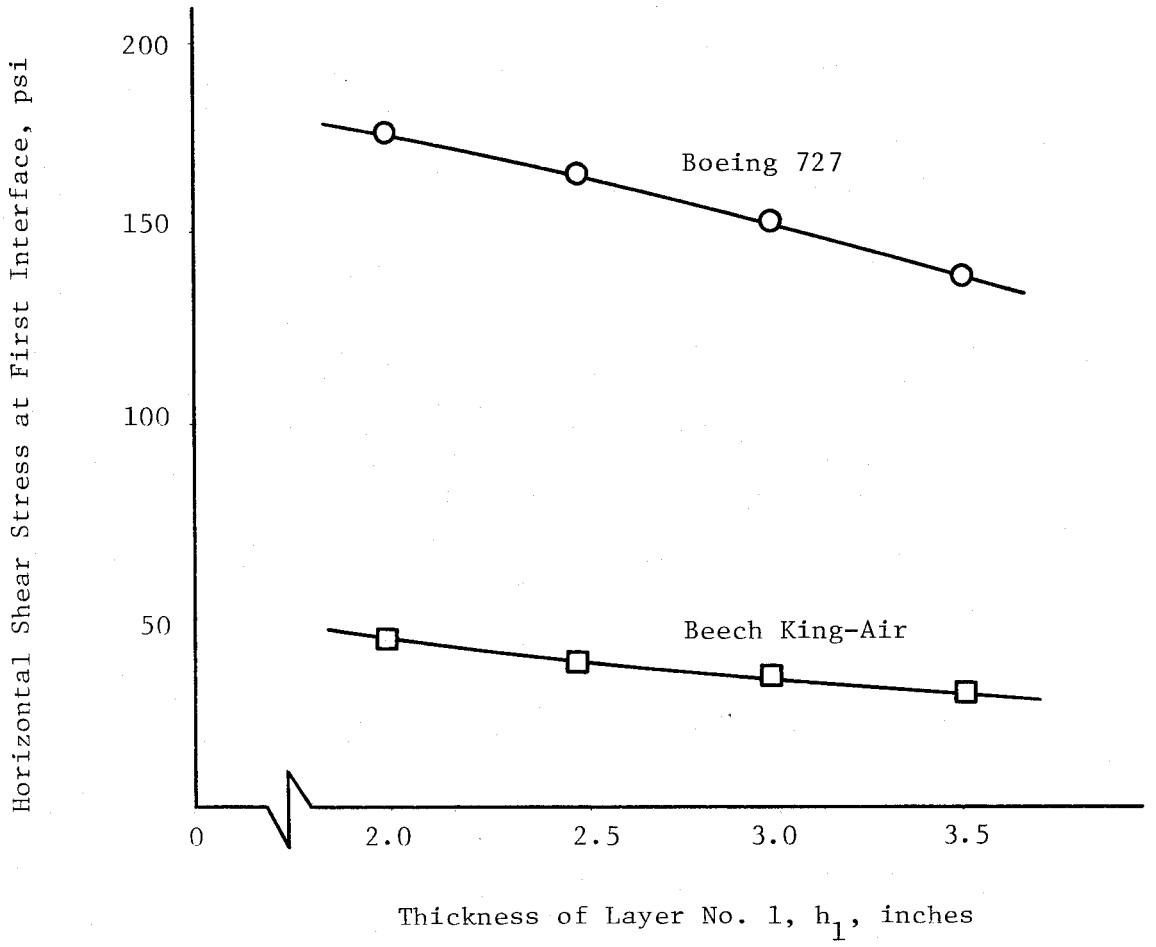

FIGURE 11. Variation in Shear Stress at First Interface due to Vertical plus Horizontal Loads (from Computer Simulation)

CONCLUSIONS

The shear strength of the interface between an asphalt concrete overlay and a simulated asphalt concrete pavement has been measured in the laboratory. The conditions duplicated by available testing equipment were that of an aircraft moving at a speed of about 25 to 30 miles per hour (40 to 48 km/hr). The vertical load applied during the test was 67 psi (4.6×10^{15} Pa). This applied pressure is similar to the tire pressure of the Beach King-Air. The shear strength of the interfaces tested at 104°F (40°C) for the fabric and non-fabric overlay systems were nearly identical and were about 15 percent below the shear strength of the asphalt concrete control specimens.

The shear stress due to a braking Boeing 727 and Beech King-Air were determined at the interface between an overlay and an old pavement. Pavement material properties were assumed to simulate an aircraft moving at about 30 miles per hour (48 km/hr) on a pavement at approximately 85°F (30°C). Shear stresses at the interfaces were of the order of 140 to 180 psi (10^6 Pa) for the Boeing 727 and of the order of 30 to 45 psi (2.5×10^5 Pa) for the Beech King-Air for pavement overlay thicknesses of 2 to 3.5 inches (5.1 to 8.9 cm).

From the above information it is evident that slippage is not likely when a Beech King-Air uses an overlaid pavement as the shear strength of the interface at 85°F (30°C) is in excess of the shear stress produced by the aircraft traveling at 30 miles per hour (48 km/hr).

Using the same logic, one would expect slippage on overlaid airfields with Boeing 727 traffic as the shear stresses created by a braking Boeing 727

aircraft are of the order of twice that of the shear strength of the interface. Experience, however, has indicated that slippage will occur only occasionally. The difference between the observed and the predicted frequency of distress is due to several factors which were not investigated in this very limited study. The factors are briefly outlined below:

1. The vertical stress applied during the test to determine the shear strength of the interface was almost one-third that applied by this aircraft. Thus, a lower shear strength was measured than would exist on the airfields.

2. In order for slippage to occur the following must occur:

   a. The shear stress produced by a braking aircraft tire must be in excess of the shear strength of the interface.

   b. The tensile strength of the overlay must be exceeded to produce the type of failure as shown in Figure 1 (i.e., the crack behind the braking aircraft).

   c. The shear strength of the overlay must be exceeded to produce the type of failure as shown in Figure 1 (i.e., the crack along the side of the tire of the braking aircraft).

   d. The compressive strength of the overlay must be exceeded to produce the type of failure as shown in Figure 1 (i.e., the shoved area in front of the braking aircraft).

It is apparent from the above discussion that prediction of slippage is a complex problem. Tools are available however, that could be used to predict this type of distress provided an extensive research program were undertaken. However, the detailed analyses are not to be attempted as part of this research program.

From the data presented and the above discussion, the following conclusions appear warranted:

1. Shear stresses at the overlay-to-old-pavement interface are primarily a function of the imposed load and tire pressure (type of aircraft) and the thickness of the overlay.

2. The probability of slippage is higher when the shear strength, tensile strength and compressive strength of the asphalt concrete are at a minimum, which occurs at high temperatures.

3. The shear strength of the Mirafi fabric and non-fabric overlay systems are nearly identical at high temperatures.

4. It is probable that no fewer or no more slippage failures would be expected for the Mirafi fabric overlaid systems than for non-fabric overlaid systems.

REFERENCES

1. Vallerga, B. A., "Asphalt Paving Mixtures - Properties, Design and Performance", course notes prepared by C. L. Monismith for a short course in Asphalt Paving Technology, 1961 - 1962, University of California, Berkeley.

2. Barenberg, E. J., Bartholomew, C. L. and Herring, M., "Pavement Distress Identification and Repair", Technical Report P-6, Construction Engineering Research Laboratory, Department of the Army, Champaign, Illinois.

3. Button, J. W., Epps, J. A., Gallaway, B. M., "Test Results on Laboratory Standard Asphalt, Aggregates and Mixtures", Texas Transportation Institute, Texas A&M University, 1977.

4. Annual Book of Standards, Part 15, Road and Paving Materials; Bituminous Materials for Highway Construction, Waterproofing, and Roofing and Pipe; Skid Resistance, American Society for Testing and Materials, 1977.

5. Standard Specifications for Transportation Materials and Methods of Sampling and Testing, Part II, American Association of State Highway and Transportation Officials, 1974.

6. Manual of Testing Procedures, Vol. 1, Texas State Department of Highways and Public Transportation, 1970.

7. Hveem, F. M., "Establishing the Oil Content for Dense-Graded Bituminous Mixtures", California Highways and Public Works, July-August, 1942.

8. Schmidt, R. J., "A Practical Method for Measuring the Resilient Modulus of Asphalt-Treated Mixes", Highway Research Record No. 404, Highway Research Board, 1972, pp. 22-32.

9. Hadley, W. O., Hudson, W. R., Kennedy, T. W., "Evaluation and Prediction of the Tensile Properties of Asphalt-Treated Materials", Research Report No. 98-9, Center for Highway Research, University of Texas at Austin, May, 1971, pp. 63-76.

10. "Mirafi 140 Fabric for Ground Stabilization and Drainage Applications", TBM-1, Celanese Fibers Marketing Co., 1974.

11. Epps, Jon A., and Button, Joe W., "Mirafi Fabric Tack Coat Requirements", Research Report RF3424-1, Texas Transportation Institute, Texas A&M University, for Celanese Fibers Marketing Co., 1977.

12. Heukelom, W., "Observations on the Rheology and Fracture of Bitumens and Asphalt Mixes", Proceedings of the Association of Asphalt Paving Technologists, Volume 35, 1966.

13. Troxell, G. E., Davis, H. E. and Kelly, J. W., Composition and Properties of Concrete, Second Edition, McGraw-Hill Book Company, 1960.

14. Nielson, J. P., "Rational Pavement Evaluation - Review of Present Technology", Technical Report No. AFWL - TR - 69-9, Air Force Weapons Laboratory, October, 1969.

15. Harrison, W. J., Wardle, J. J., Gerrard, C. M., "Computer Programs for Circle and Strip Loads on Layered, Anisotropic Media", Division of Applied Geomechanics, Commonwealth Scientific and Industrial Research Organization, Australia, 1972.

APPENDIX A

Description of Materials

TABLE A1. Characteristics of Laboratory Standard Asphalt

Characteristic Measured	Test Designation	Test Results
Relative Viscosity, 77°F (25°C)	TEX-527-C	5.8×10^5 poises
Absolute Viscosity, 140°F (60°C)	ASTM D-2171	1576 poises
Absolute Viscosity, 275°F (135°C)	AASHTO T-202	3.76 poises
Penetration, 77°F (25°C)	ASTM D-5	118 dmm
Penetration, 39.2°F (4°C)	AASHTO T-49	26 dmm
Softening Point, Ring and Ball	ASTM D-36 AASHTO T-53	107°F (42°C)
Penetration Index	Shell Method	+ 0.25
Specific Gravity, 77°F (25°C)	ASTM D-70 AASHTO T-28	1.020
Ductility, 77°F (25°C)	ASTM D-113 AASHTO T-44	150+ cm
Solubility in Trichloroethylene	ASTM D-2042 AASHTO T-44	99.9%
Flash Point and Fire Point	ASTM D-92 AASHTO T-48	615°F (324°C) 697°F (370°C)
Spot Test	AASHTO T-102	Negative
Thin Film Oven Test Penetration of Residue, 77°F Ductility of Residue, 77°F	ASTM D-1754 AASHTO T-179	68 dmm 150+ cm
Hardening Index	Actinic Light Hardening Test	1.9
Vanadium Content	Thermal Neutron Activation Analysis	3.46 $\pm$ 0.3 ppm

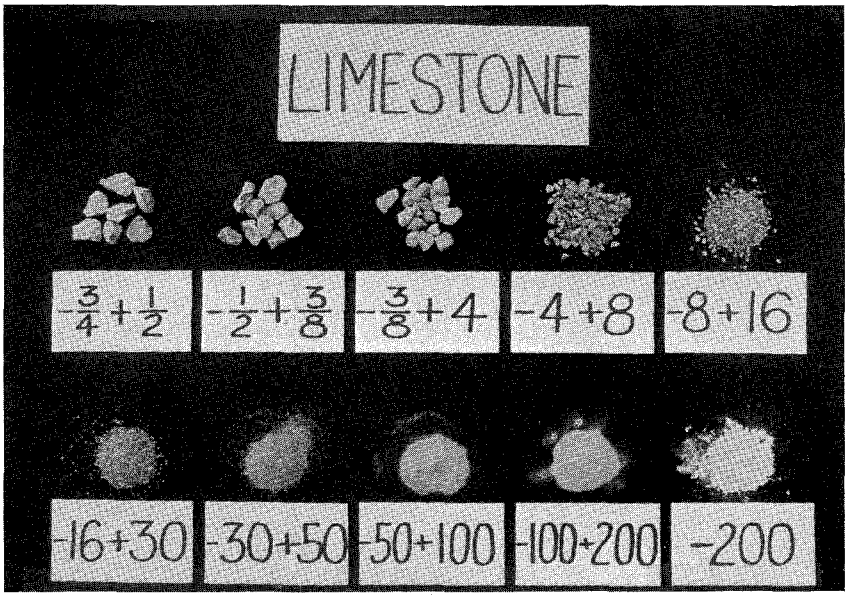

FIGURE A1. Photograph Showing Size and Shape of Standard Crushed Limestone Aggregate

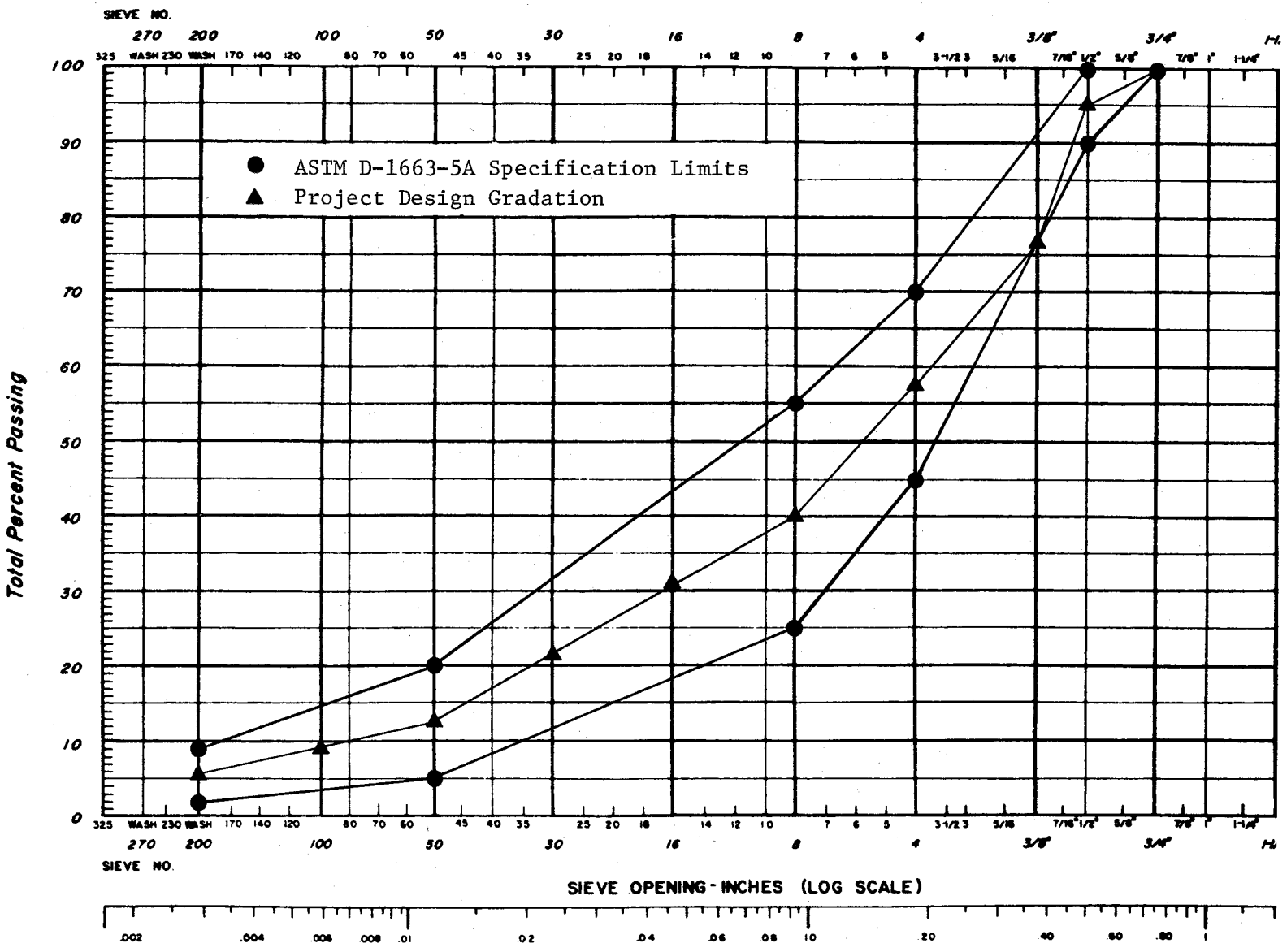

FIGURE A2. ASTM D-3515 - Aggregate Gradation 5A Specification and Project Gradation Design

TABLE A2. Physical Properties of Crushed Limestone

Physical Property	Test Designation	Aggregate Grading	Test Results
Bulk Specific Gravity	ASTM C 127 AASHTO T 85	Coarse Material*	2.663
Bulk Specific Gravity (SSD)			2.678
Apparent Specific Gravity			2.700
Absorption, percent			0.7
Bulk Specific Gravity	ASTM C 128 AASHTO T 84	Fine Material**	2.537
Bulk Specific Gravity (SSD)			2.597
Apparent Specific Gravity			2.702
Absorption, percent			2.2
Bulk Specific Gravity	ASTM C 127 & C 128 AASHTO T 84 & T 85	Project Design Gradation	2.589
Apparent Specific Gravity			2.701
Absorption, percent			1.56
Abrasion Resistance, percent loss	ASTM C 131 AASHTO T 96	Grading C	23
Compacted Unit Weight, pcf	ASTM C 29 AASHTO T 19	Project Design Gradation	122
Surface Capacity, percent by wt. dry aggregate	Centrifuge Kerosene Equivalent	Fine Material**	4.1
Surface Capacity, percent by wt. dry aggregate	Oil Equivalent	-3/8 inch to + No. 4	2.3
Estimated Optimum Asphalt Content, percent by wt. dry aggregate	C.K.E. and Oil Equivalent	Project Design Gradation	5.5

*Material retained on No. 4 sieve from Project Design Gradation

**Material passing No. 4 sieve from Project Design Gradation

TABLE A3. Mixture Properties of Limestone plus APP AC-10 at Optimum Asphalt Content

Property	Crushed Limestone
Design Asphalt Content, percent by wt. aggregate	4.5
Marshall Specimens	
Unit Weight, pcf	153
Air Void Content, percent	3.0
VMA, percent	10.5
VMA Filled w/Asphalt, percent	78
Marshall Stability, lb	2740
Marshall Flow, .01 inch	11
Hveem Specimens	
Unit Weight, pcf	154
Air Void Content, percent	2.5
VMA, percent	9.1
VMA Filled w/Asphalt, percent	81
Hveem Stability, percent	54
Resilient Modulus @68°F, psi	590,000
Elastic Modulus @ Failure at 68°F *, psi	26,000

* From Splitting Tensile Test

APPENDIX B

Results of Computer Simulation Study

TABLE B1. Pavement Stresses for Boeing 727 on 2.0-inch Overlay

Pavement Depth, in.	Radius, in.	Stress @ 0°		Stress @ 180°	
		Vert., psi	Horiz., psi	Vert., psi	Horiz., psi
0	0.00	168	132	168	132
	4.35	168	132	168	132
	7.5	168	132	168	132
	8.7	168	132	168	132
	8.8	0	0	0	0
	13.05	0	0	0	0
	17.4	0	0	0	0
	26.1	0	0	0	0
1.75	0	141	54	141	54
	4.35	140	120	134	0
	7.5	139	158	99	-83
	8.7	101	178	39	-96
	8.8	95	178	34	-94
	13.05	10	77	5	-35
	17.4	4	34	2	-17
	26.1	1	11	0	- 7
1.9	0	137	49	137	49
	4.35	136	106	129	-18
	7.5	134	157	93	-89
	8.7	98	177	39	-99
	8.8	93	177	34	-97
	13.05	12	79	5	-36
	17.4	5	35	2	-18
	26.1	1	12	0	- 7
2.0	0	134	45	134	45
	4.35	133	102	126	-22
	7.5	130	156	90	-92
	8.7	95	175	38	-100
	8.8	91	175	34	-99
	13.05	13	80	6	-37
	17.4	5	36	2	-18
	26.1	1	12	0	- 8

TABLE B1. (Continued)

Pavement Depth, in.	Radius, in.	Stress @ 0°		Stress @ 180°	
		Vert., psi	Horiz., psi	Vert., psi	Horiz., psi
2.5	0.00	120	30	120	30
	4.35	119	88	109	-37
	7.5	110	144	74	-99
	8.7	84	161	38	-101
	8.8	81	161	35	-99
	13.05	18	81	8	-38
	17.4	7	37	3	-20
	26.1	1	14	1	- 9
3.0	0.00	108	18	108	18
	4.35	106	70	70	-41
	7.5	93	120	61	-91
	8.7	74	134	38	-91
	8.8	72	135	36	-90
	13.05	22	73	10	-37
	17.4	8	37	4	-20
	26.1	1	15	1	-10
3.5	0.00	97	8	97	8
	4.35	94	48	80	-35
	7.5	78	84	52	-69
	8.7	65	95	37	-68
	8.8	64	95	36	-67
	13.05	25	58	12	-31
	17.4	9	33	4	-20
	26.1	2	15	1	-10
4.0	0.00	90	1.2	90	- 1
	4.35	87	22	73	-19
	7.5	70	36	47	-29
	8.7	60	39	36	-30
	8.8	59	39	36	-30
	13.05	26	35	12	-33
	17.4	10	26	4	-18
	26.1	2	15	1	-10

TABLE B2. Pavement Stresses for Boeing 727 on 2.5-inch Overlay

Pavement Depth, in.	Radius in.	Stress @ 0°		Stress @ 180°	
		Vert., psi	Horiz., psi	Vert., psi	Horiz., psi
0	0.00	168	132	168	132
	4.35	168	132	168	132
	7.5	168	132	168	132
	8.7	168	132	168	132
	8.8	0	0	0	0
	13.05	0	0	0	0
	17.4	0	0	0	0
	26.1	0	0	0	0
1.75	0.00	142	57	142	57
	4.35	143	111	138	- 5
	7.5	143	154	100	-74
	8.7	103	173	38	-87
	8.8	97	173	33	-86
	13.05	8	77	3	-35
	17.4	4	36	2	-18
	26.1	1	12	0	- 7
1.9	0.00	138	52	138	52
	4.35	139	108	133	-13
	7.5	138	155	95	-80
	8.7	100	173	37	-91
	8.8	95	173	33	-90
	13.05	10	80	4	-37
	17.4	4	38	2	-19
	26.1	1	13	0	- 8
2.0	0.00	135	49	135	-49
	4.35	136	106	129	-17
	7.5	134	154	91	-84
	8.7	98	172	37	-93
	8.8	93	172	33	-92
	13.05	11	82	4	-38
	17.4	5	39	2	-19
	26.1	1	13	0	- 8

TABLE B2. (Continued)

Pavement Depth, in.	Radius in.	Stress @ 0°		Stress @ 180°	
		Vert., psi	Horiz., psi	Vert., psi	Horiz., psi
2.5	0.00	121	34	121	34
	4.35	122	94	113	-34
	7.5	116	148	75	-95
	8.7	87	164	36	-98
	8.8	84	164	33	-97
	13.05	15	86	6	-40
	17.4	6	41	3	-21
	26.1	1	15	1	- 9
3.0	0.00	107	22	107	22
	4.35	107	80	96	43
	7.5	98	133	63	95
	8.7	97	147	35	95
	8.8	74	147	33	84
	13.05	19	83	9	40
	17.4	8	41	4	22
	26.1	1	16	1	10
3.5	0.00	95	12	95	12
	4.35	94	62	82	-43
	7.5	82	108	53	-84
	8.7	67	120	35	-83
	8.8	65	121	33	-82
	13.05	22	72	11	-37
	17.4	10	38	4	-21
	26.1	2	16	1	-10
4.0	0.00	85	5	85	5
	4.35	83	42	70	-35
	7.5	70	75	46	-62
	8.7	59	83	34	-61
	13.05	25	55	12	-31
	17.4	11	33	5	-20
	26.1	2	16	1	-10

TABLE B3. Pavement Stresses for Boeing 727 on 3.0-inch Overlay

Pavement Depth, in.	Radius in.	Stress @ 0°		Stress @ 180°	
		Vert., psi	Horiz., psi	Vert., psi	Horiz., psi
0	0.00	168	132	168	132
	4.35	168	132	168	132
	7.5	168	132	168	132
	8.7	168	132	168	132
	8.8	0	0	0	0
	13.05	0	0	0	0
	17.4	0	0	0	0
	26.1	0	0	0	0
1.75	0.00	143	60	143	60
	4.35	145	110	140	- 2
	7.5	146	149	101	-64
	8.7	104	167	37	-78
	8.8	99	167	32	-78
	13.05	7	76	2	-34
	17.4	3	38	2	-19
	26.1	1	13	0	- 8
1.9	0.00	140	55	140	55
	4.35	142	109	136	6
	7.5	141	150	96	71
	8.7	101	167	37	83
	8.8	96	167	32	82
	13.05	8	79	3	36
	17.4	4	39	2	20
	26.1	9	14	0	8
2.0	0.00	137	52	137	52
	4.35	139	107	133	10
	7.5	138	150	92	75
	8.7	100	167	36	85
	8.8	95	167	32	84
	13.05	9	81	3	37
	17.4	4	40	2	20
	26.1	1	14	0	14

TABLE B3. (Continued)

Pavement Depth, in.	Radius in.	Stress @ 0°		Stress @ 180°	
		Vert., psi	Horiz., psi	Vert., psi	Horiz., psi
2.5	0.00	123	38	123	38
	4.35	123	97	120	-30
	7.5	120	147	77	-89
	8.7	90	162	35	-93
	8.8	86	163	32	-92
	13.05	12	87	5	-41
	17.4	6	44	3	-22
	26.1	1	16	1	-10
3.0	0.00	109	26	109	26
	4.35	111	86	101	-41
	7.5	103	137	64	-93
	8.7	79	151	34	-94
	8.8	77	151	31	-93
	13.05	16	88	7	-42
	17.4	8	45	4	-23
	26.1	2	17	1	-10
3.5	0.00	96	16	96	16
	4.35	97	72	86	-46
	7.5	86	121	54	-89
	8.7	69	133	33	-88
	8.8	67	133	31	-87
	13.05	20	82	9	-41
	17.4	9	43	4	-23
	26.1	2	17	1	-11
4.0	0.00	84	8	84	8
	4.35	84	56	72	-43
	7.5	73	97	46	-77
	8.7	60	107	32	-75
	8.8	55	108	31	-75
	13.05	22	70	11	-75
	17.4	10	39	5	-36
	26.1	3	17	1	-22

TABLE B4. Pavement Stresses for Boeing 727 on 3.5-inch Overlay

Pavement Depth, in.	Radius in.	Stress @ 0°		Stress @ 180°	
		Verts., psi	Horiz., psi	Vert., psi	Horiz., psi
0	0.00	168	132	168	132
	4.35	168	132	168	132
	7.5	168	132	168	132
	8.7	168	132	168	132
	8.8	0	0	0	0
	31.05	0	0	0	0
	17.4	0	0	0	0
	26.1	0	0	0	0
1.75	0.00	145	63	145	63
	4.35	148	110	143	8
	7.5	149	144	102	-55
	8.7	106	160	37	-71
	8.8	100	160	31	-70
	13.05	6	73	1	-32
	17.4	3	38	1	-19
	26.1	1	14	0	- 8
1.9	0.00	142	58	142	58
	4.35	145	108	139	1
	7.5	144	145	97	-62
	8.7	104	161	36	-75
	8.8	98	161	31	-74
	13.05	7	77	2	-34
	17.4	3	40	2	-20
	26.1	1	15	0	- 8
2.0	0.00	140	55	139	55
	4.35	142	106	136	- 3
	7.5	141	145	93	-66
	8.7	101	161	36	-77
	8.8	96	161	31	-76
	13.05	7	79	2	-35
	17.4	4	41	2	-21
	26.1	1	15	0	- 9

TABLE B4. (Continued)

Pavement Depth, in.	Radius in.	Stress @ 0°		Stress @ 180°	
		Vert., psi	Horiz., psi	Vert., psi	Horiz., psi
2.5	0.00	126	41	126	41
	4.35	130	98	121	24
	7.5	125	144	78	-81
	8.7	92	158	34	-86
	8.8	88	158	31	-85
	13.05	10	87	3	-40
	17.4	5	46	3	-23
	26.1	1	17	1	-10
3.0	0.00	113	29	113	29
	4.35	116	88	106	-37
	7.5	108	138	66	-89
	8.7	82	150	33	-90
	8.8	79	151	30	-89
	13.05	14	89	5	-42
	17.4	7	47	3	-24
	26.1	2	18	1	-11
3.5	0.00	99	19	99	19
	4.35	101	77	90	-45
	7.5	92	126	56	-89
	8.7	72	138	31	-88
	8.8	70	138	29	-87
	13.05	17	87	7	-42
	17.4	8	47	4	-25
	26.1	2	19	1	-11
4.0	0.00	86	11	96	11
	4.35	87	65	76	-47
	7.5	77	110	47	-83
	8.7	63	120	30	-81
	8.8	61	120	29	-81
	13.05	20	79	9	-40
	17.4	10	44	5	-24
	26.1	3	19	1	-12

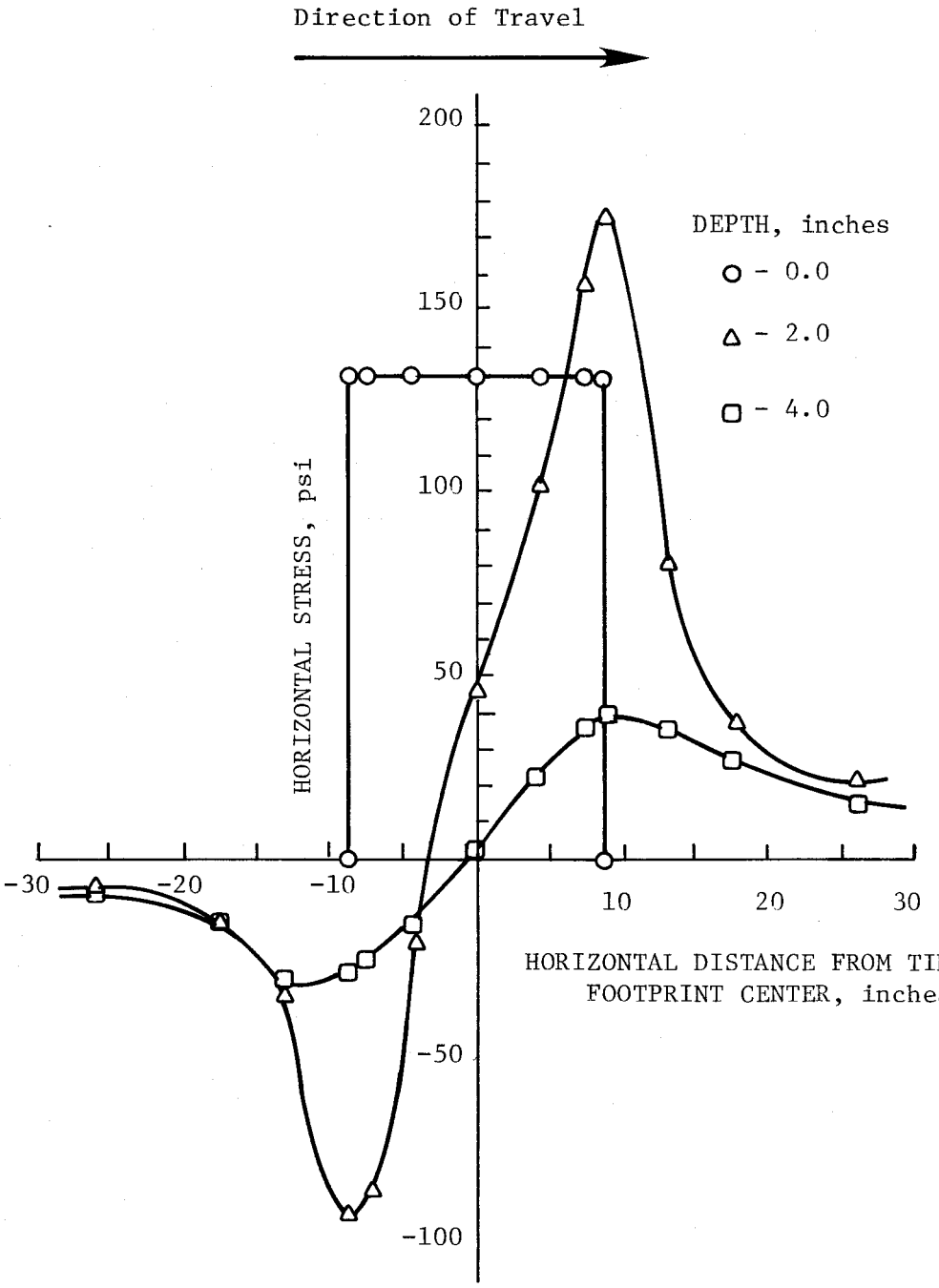

FIGURE B1. Horizontal Stress Distribution for Boeing 727 on 2.0-inch Overlay

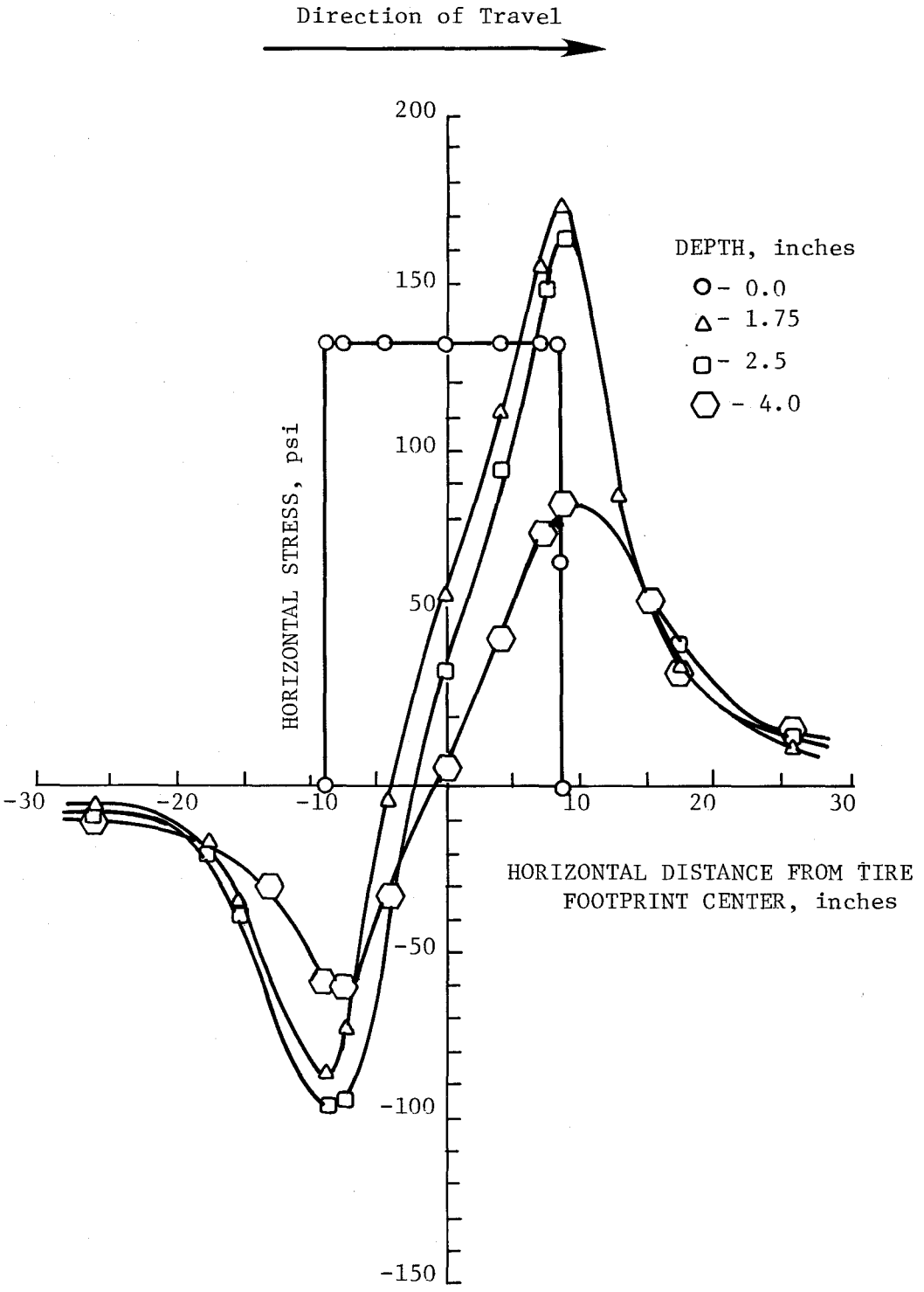

FIGURE B2. Horizontal Stress Distribution for Boeing 727 on 2.5-inch Overlay

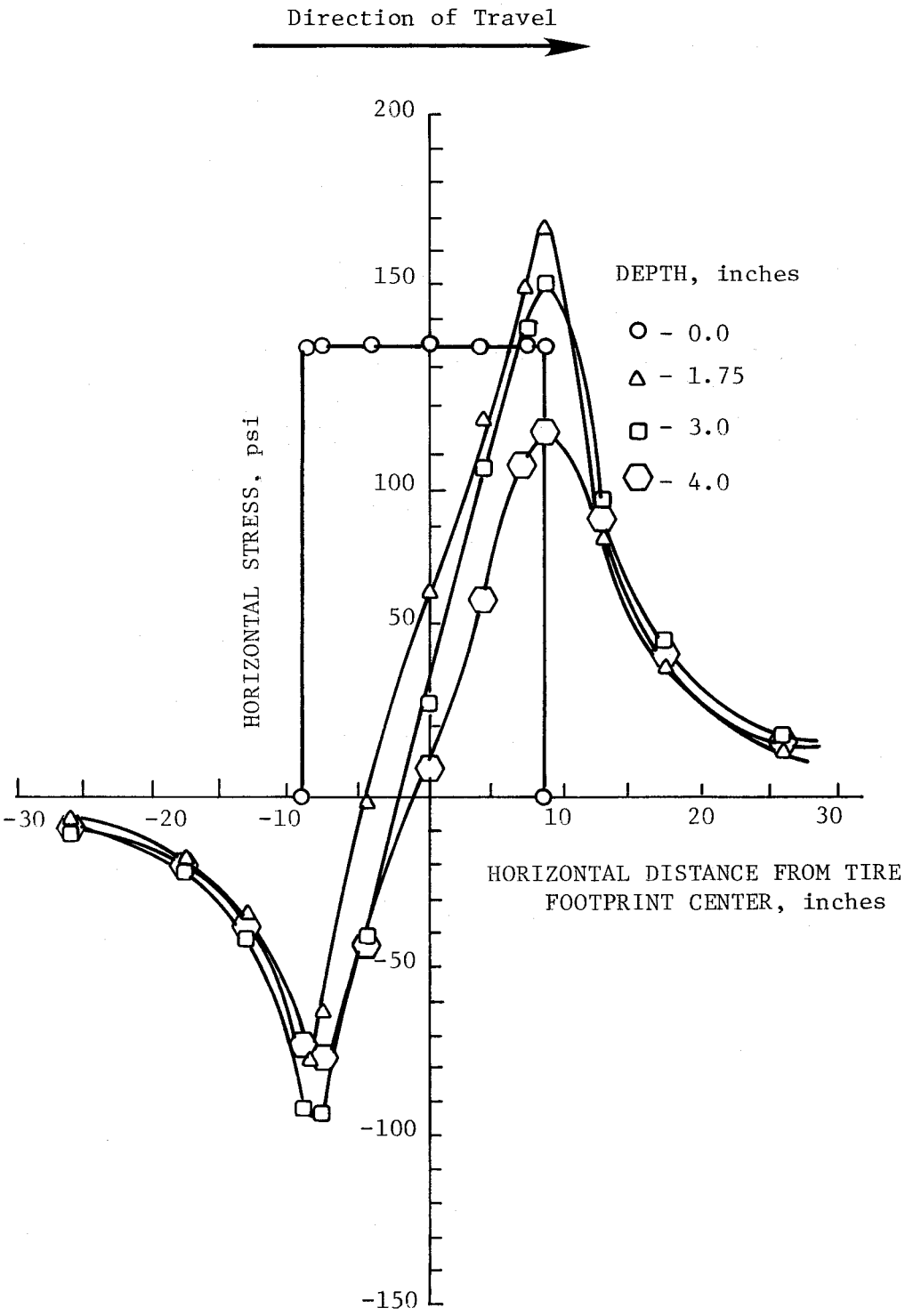

FIGURE B3. Horizontal Stress Distribution for Boeing 727 on 3.0-inch Overlay

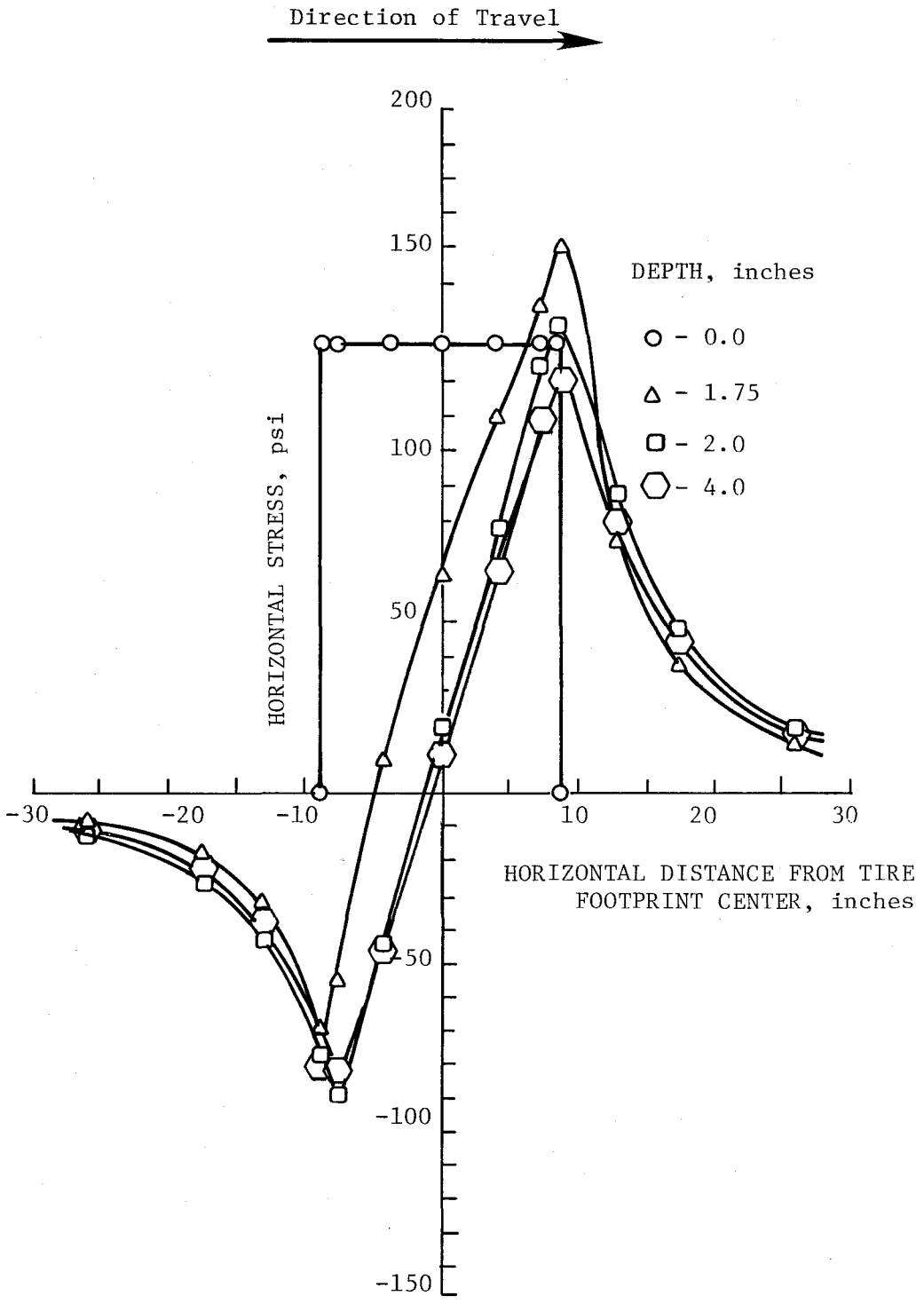

FIGURE B4. Horizontal Stress Distribution for Boeing 727 on 3.5-inch Overlay

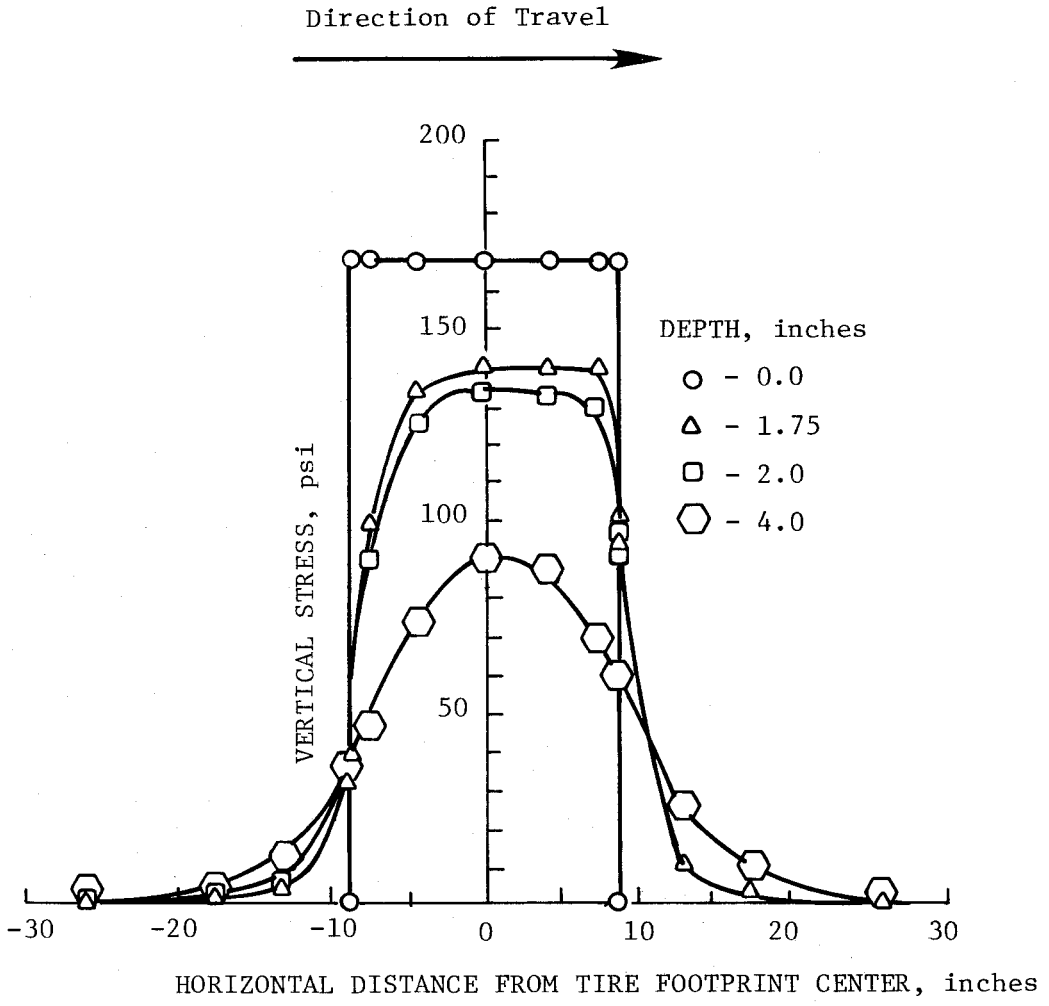

FIGURE B5. Vertical Stress Distribution for Boeing 727 on 2.0-inch Overlay

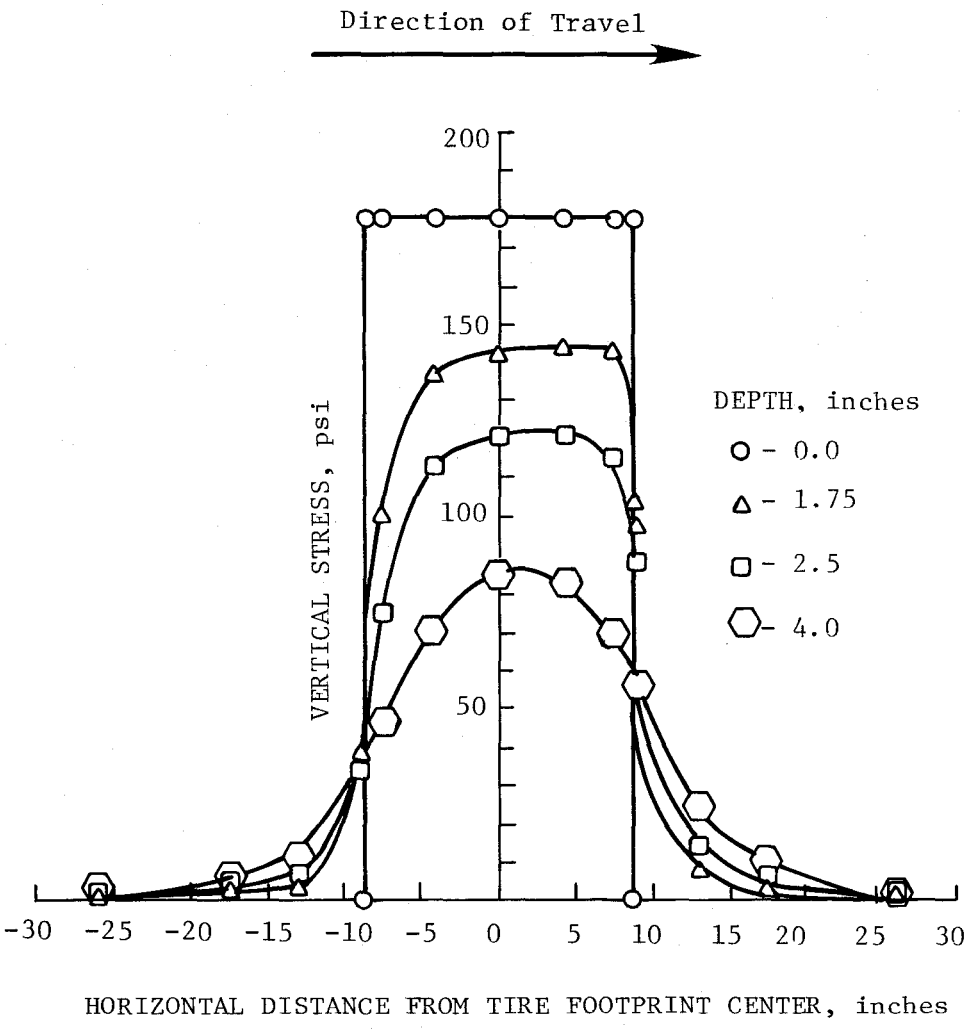

FIGURE B6. Vertical Stress Distribution for Boeing 727 on 2.5-inch Overlay

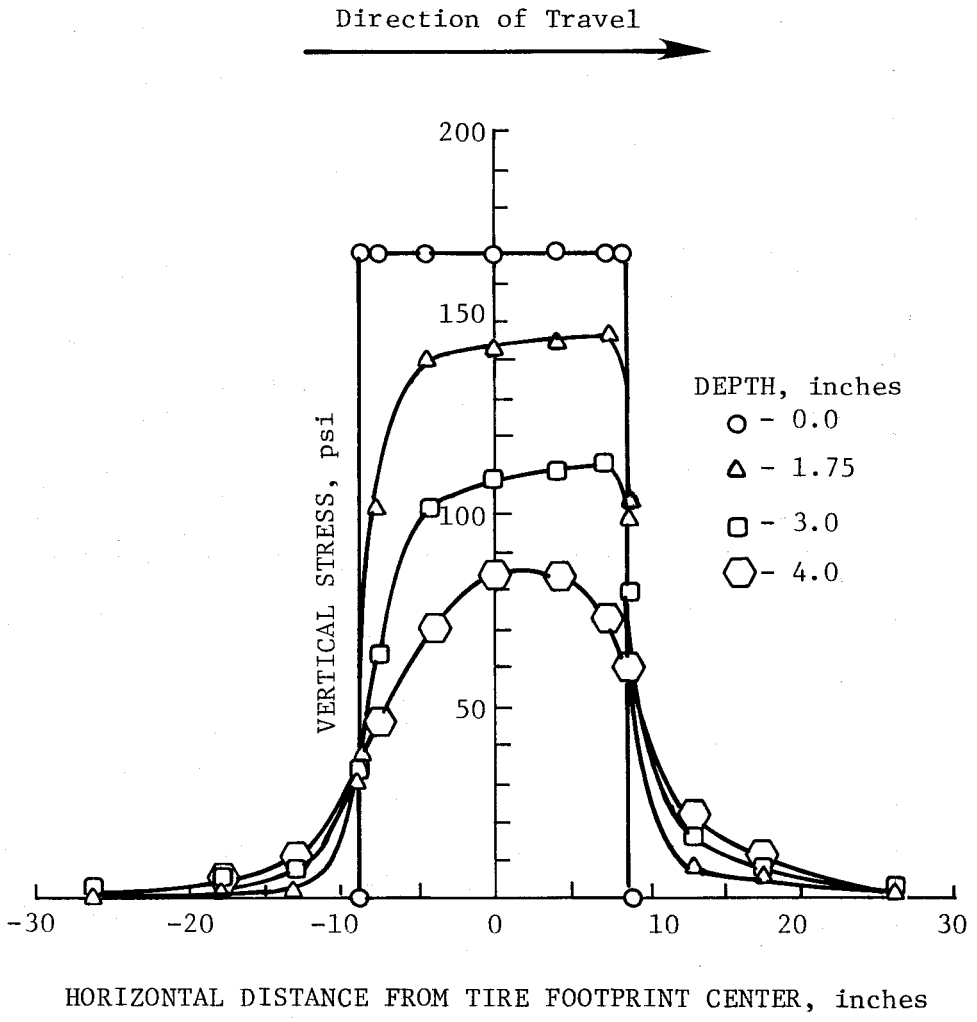

FIGURE B7. Vertical Stress Distribution for Boeing 727 on 3.0-inch Overlay

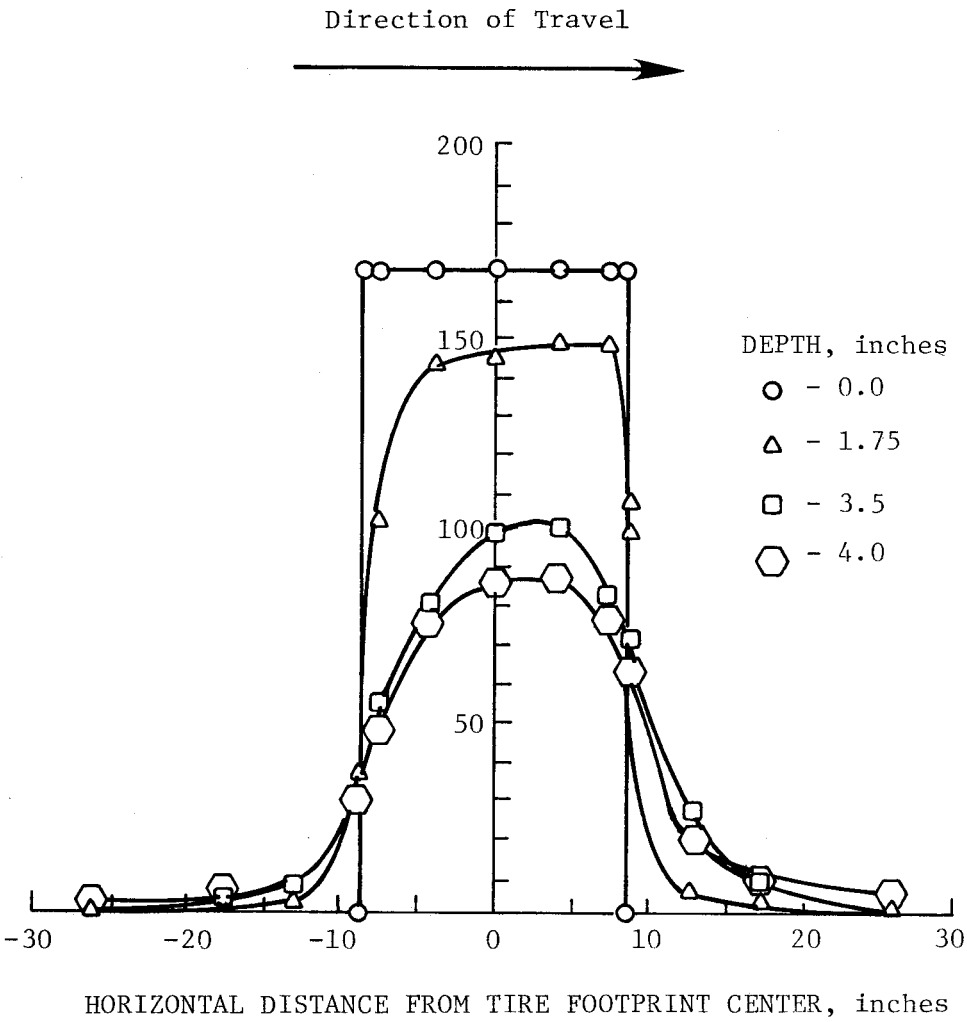

FIGURE B8. Vertical Stress Distribution for Boeing 727 on 3.5-inch Overlay

TABLE B5. Pavement Stresses for Beechcraft King-Air on 2.0-inch Overlay

Pavement Depth, in.	Radius in.	Stress @ 0°		Stress @ 180°	
		Vert., psi	Horiz., psi	Vert., psi	Horiz., psi
0	0.00	52	42	52	42
	2.65	52	42	52	42
	4.35	52	42	52	42
	5.3	52	42	52	42
	7.5	0	0	0	0
	8.7	0	0	0	0
	8.8	0	0	0	0
	13.05	0	0	0	0
	17.4	0	0	0	0
	26.1	0	0	0	0
1.75	0.00	39	13	39	13
	2.65	41	38	37	9
	4.35	40	39	36	-19
	5.3	30	44	11	-22
	7.5	5	29	0	-10
	8.7	3	21	1	- 8
	8.8	3	21	1	- 8
	13.05	1	8	0	- 3
	17.4	0	3	0	- 2
	26.1	0	1	0	- 1
1.90	0.00	37	11	37	11
	2.65	39	27	35	- 7
	4.35	29	38	24	-20
	5.3	28	43	11	-22
	7.5	5	29	1	-12
	8.7	3	22	1	- 9
	8.8	3	21	1	- 8
	13.05	1	8	1	- 3
	17.4	0	4	0	- 2
	26.1	0	1	0	- 1

TABLE B5. (Continued)

Pavement Depth, in.	Radius in.	Stress @ 0°		Stress @ 180°	
		Vert., psi	Horiz., psi	Vert., psi	Horiz., psi
2.0	0.00	36	10	36	10
	2.65	38	26	34	-8
	4.35	36	38	23	-21
	5.3	27	43	10	-23
	7.5	6	30	1	-12
	8.7	3	22	1	-9
	8.8	3	21	1	-8
	13.05	1	8	1	-4
	17.4	0	4	0	-2
	26.1	0	1	0	-1
2.5	0.00	30	5	30	5
	2.65	31	22	27	-12
	4.35	29	34	18	-22
	5.3	23	38	10	-23
	7.5	6	29	2	-12
	8.7	5	21	2	-9
	8.8	5	21	2	-9
	13.05	2	8	1	-4
	17.4	1	4	0	-2
	26.1	0	2	0	-1
3.0	0.00	24	2	24	2
	2.65	25	17	21	-13
	4.35	23	27	14	-20
	5.3	18	31	9	-20
	7.5	8	34	3	-11
	8.7	6	19	3	-8
	8.8	6	18	3	-8
	13.05	2	8	1	-4
	17.4	1	4	0	-2
	26.1	0	2	0	-1

TABLE B5. (Continued)

Pavement Depth, in.	Radius in.	Stress @ 0°		Stress @ 180°	
		Vert., psi	Horiz., psi	Vert., psi	Horiz., psi
3.5	0.00	19	0	19	0
	2.65	20	11	16	-10
	4.35	18	18	12	-15
	5.3	15	20	8	-14
	7.5	9	17	4	- 9
	8.7	7	13	3	- 6
	8.8	6	13	3	- 6
	13.05	2	5	1	- 3
	17.4	1	4	0	- 2
	26.1	0	2	0	- 1
4.0	0.00	17	0	17	0
	2.65	17	3	14	- 3
	4.35	15	5	10	- 4
	5.3	13	6	8	- 5
	7.5	9	6	5	- 4
	8.7	7	6	3	- 4
	8.8	7	6	3	- 4
	13.05	3	4	1	- 3
	17.4	1	3	0	- 2
	26.1	0	2	0	- 1

TABLE B6. Pavement Stresses for Beechcraft King-Air on 2.5-inch Overlay

Pavement Depth, in.	Radius in.	Stress @ 0°		Stress @ 180°	
		Vert., psi	Horiz., psi	Vert., psi	Horiz., psi
0	0.00	52	42	52	42
	2.65	52	42	52	42
	4.35	52	42	52	42
	5.3	52	42	52	42
	7.5	0	0	0	0
	8.7	0	0	0	0
	8.8	0	0	0	0
	13.05	0	0	0	0
	17.4	0	0	0	0
	26.1	0	0	0	0
1.75	0.00	41	14	41	14
	2.65	43	28	39	2
	4.35	41	37	11	-16
	5.3	31	42	11	-19
	7.5	4	37	0	-10
	8.7	2	20	0	- 8
	8.8	2	20	0	- 8
	13.05	1	8	0	- 4
	17.4	0	4	0	- 2
	26.1	0	1	0	- 1
1.90	0.00	39	12	39	12
	2.65	41	27	37	- 4
	4.35	39	37	25	-17
	5.3	29	42	11	-20
	7.5	5	28	0	-10
	8.7	3	21	1	- 8
	8.8	2	20	1	- 8
	13.05	1	8	1	- 4
	17.4	0	4	0	- 2
	26.1	0	1	0	- 1

TABLE B6. (Continued)

Pavement Depth, in.	Radius in.	Stress @ 0°		Stress @ 180°	
		Vert., psi	Horiz., psi	Vert., psi	Horiz., psi
2.0	0.00	38	11	38	11
	2.65	40	26	36	- 6
	4.35	38	37	24	-26
	5.3	28	41	10	-20
	7.5	5	28	0	-11
	8.7	3	21	1	- 8
	8.8	3	21	1	- 8
	13.05	1	9	1	- 4
	17.4	0	4	0	- 2
	26.1	0	1	0	- 1
2.5	0.00	32	7	32	7
	2.65	34	23	29	-11
	4.35	31	34	19	-21
	5.3	24	38	9	-21
	7.5	7	29	1	-12
	8.7	4	22	1	- 9
	8.8	4	22	1	- 9
	13.05	2	9	1	- 4
	17.4	1	4	0	- 2
	26.1	0	2	0	- 1
3.0	0.00	26	31	26	3
	2.65	27	19	23	13
	4.35	25	29	15	-21
	5.3	20	33	9	-21
	7.5	8	27	2	-12
	8.7	5	21	2	- 9
	8.8	5	20	2	- 9
	13.05	2	9	1	- 4
	17.4	1	4	0	- 2
	26.1	0	2	0	- 1

TABLE B6. (Continued)

Pavement Depth, in.	Radius in.	Stress @ 0°		Stress @ 180°	
		Vert., psi	Horiz., psi	Vert., psi	Horiz., psi
3.5	0.00	21	9	21	8
	2.65	21	14	17	12
	4.35	19	23	12	-18
	5.3	16	26	8	-18
	7.5	8	22	3	-11
	8.7	6	13	2	- 8
	8.8	6	17	2	- 8
	13.05	2	8	1	- 4
	17.4	1	4	0	- 2
	26.1	0	2	0	- 1
4.0	0.00	16	0	17	0.26
	2.65	17	9	14	- 9
	4.35	15	15	10	13
	5.3	13	17	7	12
	7.5	8	15	4	- 8
	8.7	6	12	3	- 6
	8.8	6	12	3	- 6
	13.05	3	6	1	- 3
	17.4	1	4	0	- 2
	26.1	0	2	0	- 1

TABLE B7. Pavement Stresses for Beechcraft King-Air on 3.0-inch Overlay

Pavement Depth, in.	Radius in.	Stress @ 0°		Stress @ 180°	
		Vert., psi	Horiz., psi	Vert., psi	Horiz., psi
0	0.00	52	42	52	42
	2.65	52	42	52	42
	4.35	52	42	52	42
	7.5	0	0	0	0
	8.7	0	0	0	0
	8.8	0	0	0	0
	13.05	0	0	0	0
	17.4	0	0	0	0
	26.1	0	0	0	0
1.75	0.00	43	15	43	15
	2.65	44	27	40	0
	4.35	43	36	27	-13
	5.3	31	40	11	-16
	7.5	4	26	0	- 8
	8.7	2	19	0	- 7
	8.8	2	19	0	- 7
	13.05	1	8	0	- 4
	17.4	0	4	0	- 2
	26.1	0	1	0	- 1
1.90	0.00	41	14	41	14
	2.65	43	26	38	- 2
	4.35	41	35	25	-15
	5.3	30	40	10	-17
	7.5	5	27	-1	- 9
	8.7	2	20	0	- 7
	8.8	2	20	0	- 7
	13.05	1	6	0	- 4
	17.4	0	4	0	- 2
	26.1	0	2	0	- 1

TABLE B7. (Continued)

Pavement Depth, in.	Radius in.	Stress @ 0°		Stress @ 180°	
		Vert., psi	Horiz., psi	Vert., psi	Horiz., psi
2.0	0.00	40	13	40	13
	2.65	42	26	37	- 3
	4.35	34	35	24	-16
	5.3	29	39	10	-18
	7.5	5	27	0	-10
	8.7	2	20	0	- 8
	8.8	2	20	0	- 8
	13.05	1	9	0	- 4
	17.4	0	4	0	- 2
	26.1	0	2	0	- 1
2.5	0.00	34	8	34	8
	2.65	36	23	31	- 9
	4.35	33	33	19	-19
	5.3	25	37	9	-19
	7.5	6	28	0	-11
	8.7	3	22	1	- 9
	8.8	3	21	1	- 8
	13.05	1	10	1	- 4
	17.4	1	5	0	- 2
	26.1	0	2	0	- 1
3.0	0.00	29	4	29	4
	2.65	30	20	24	-12
	4.35	27	30	16	-20
	5.3	21	33	8	-20
	7.5	7	27	1	-12
	8.7	4	21	1	- 9
	8.8	4	21	1	- 9
	13.05	2	9	1	- 4
	17.4	1	5	0	- 2
	26.1	0	2	0	- 1

TABLE B7. (Continued)

Pavement Depth, in.	Radius in.	Stress @ 0°		Stress @ 180°	
		Vert., psi	Horiz., psi	Vert., psi	Horiz., psi
3.5	0.00	23	2	23	2
	2.65	24	16	19	-13
	4.35	21	24	12	-19
	5.3	17	28	8	-18
	7.5	17	24	2	-12
	8.7	5	20	2	- 9
	8.8	5	19	2	- 8
	13.05	2	9	1	- 4
	17.4	1	5	0	- 2
	26.1	0	2	0	- 1
4.0	0.00	19	0	18	0
	2.65	19	12	15	-12
	4.35	17	20	10	-16
	5.3	14	22	7	-16
	7.5	7	20	3	-10
	8.7	5	16	2	- 8
	8.8	5	16	2	- 7
	13.05	2	8	1	- 4
	17.4	1	4	0	- 2
	26.1	0	2	0	- 1

TABLE B8. Pavement Stresses for Beechcraft King-Air on 3.5-inch Overlay

Pavement Depth in.	Radius in.	Stress @ 0°		Stress @ 180°	
		Vert., psi	Horiz., psi	Vert., psi	Horiz., psi
0	0.00	52	42	52	42
	2.65	52	42	52	42
	4.35	52	42	52	42
	5.3	52	42	52	42
	7.5	0	0	0	0
	8.7	0	0	0	0
	8.8	0	0	0	0
	13.05	0	0	0	0
	17.4	0	0	0	0
	26.1	0	0	0	0
1.75	0.00	44	16	44	16
	2.65	46	27	41	3
	4.35	44	34	27	-11
	5.3	32	39	11	-14
	7.5	4	23	- 1	- 7
	8.7	2	18	0	- 6
	8.8	2	18	0	- 6
	13.05	1	8	0	- 4
	17.4	0	4	0	- 2
	26.1	0	2	0	- 1
1.90	0.00	43	15	43	15
	2.65	45	26	39	0
	4.35	42	34	26	-12
	5.3	31	38	11	-15
	7.5	5	25	- 1	- 8
	8.7	2	19	0	- 7
	8.8	2	18	0	- 6
	13.05	1	8	0	- 4
	17.4	0	4	0	- 2
	26.1	0	4	0	- 2

TABLE B8. (Continued)

Pavement Depth, in.	Radius in.	Stress @ 0°		Stress @ 180°	
		Vert., psi	Horiz., psi	Vert., psi	Horiz., psi
2.0	0.00	42	14	42	-14
	2.65	44	25	38	- 1
	4.35	41	34	25	-13
	5.3	30	38	10	-16
	7.5	5	26	- 1	- 8
	8.7	2	19	0	- 7
	8.8	2	19	0	- 7
	13.05	1	9	0	- 4
	17.4	0	5	0	- 2
	26.1	0	2	0	- 1
2.5	0.00	37	9	37	9
	2.65	38	23	32	- 7
	4.35	35	32	20	-16
	5.3	26	36	9	-17
	7.5	6	27	0	-10
	8.7	3	21	0	- 8
	8.8	3	21	0	- 8
	13.05	1	10	1	- 4
	17.4	1	5	0	- 2
	26.1	0	2	0	- 1
3.0	0.00	31	51	31	51
	2.65	33	20	26	-10
	4.35	29	30	16	-18
	5.3	22	33	8	-18
	7.5	7	27	1	-11
	8.7	4	21	1	- 9
	8.8	4	21	1	- 9
	13.05	1	10	1	- 4
	17.4	1	5	0	- 3
	26.1	0	2	0	- 1

TABLE B8. (Continued)

Pavement Depth, in.	Radius in.	Stress @ 0°		Stress @ 180°	
		Vert., psi	Horiz., psi	Vert., psi	Horiz., psi
3.5	0.00	26	2	26	2
	2.65	27	17	21	-12
	4.35	23	26	13	-18
	5.3	19	29	8	-18
	7.5	7	25	1	-12
	8.7	4	20	1	- 9
	8.8	4	20	1	- 9
	13.05	2	10	1	- 4
	17.4	1	5	0	- 3
	26.1	0	2	0	- 1
4.0	0.00	20	0	20	0
	2.65	21	14	17	-12
	4.35	19	22	11	-17
	5.3	15	25	7	-17
	7.5	7	22	2	-11
	8.7	5	18	2	- 8
	8.8	5	18	2	- 8
	13.05	2	9	1	- 4
	17.4	1	5	0	- 3
	26.1	0	2	0	- 1

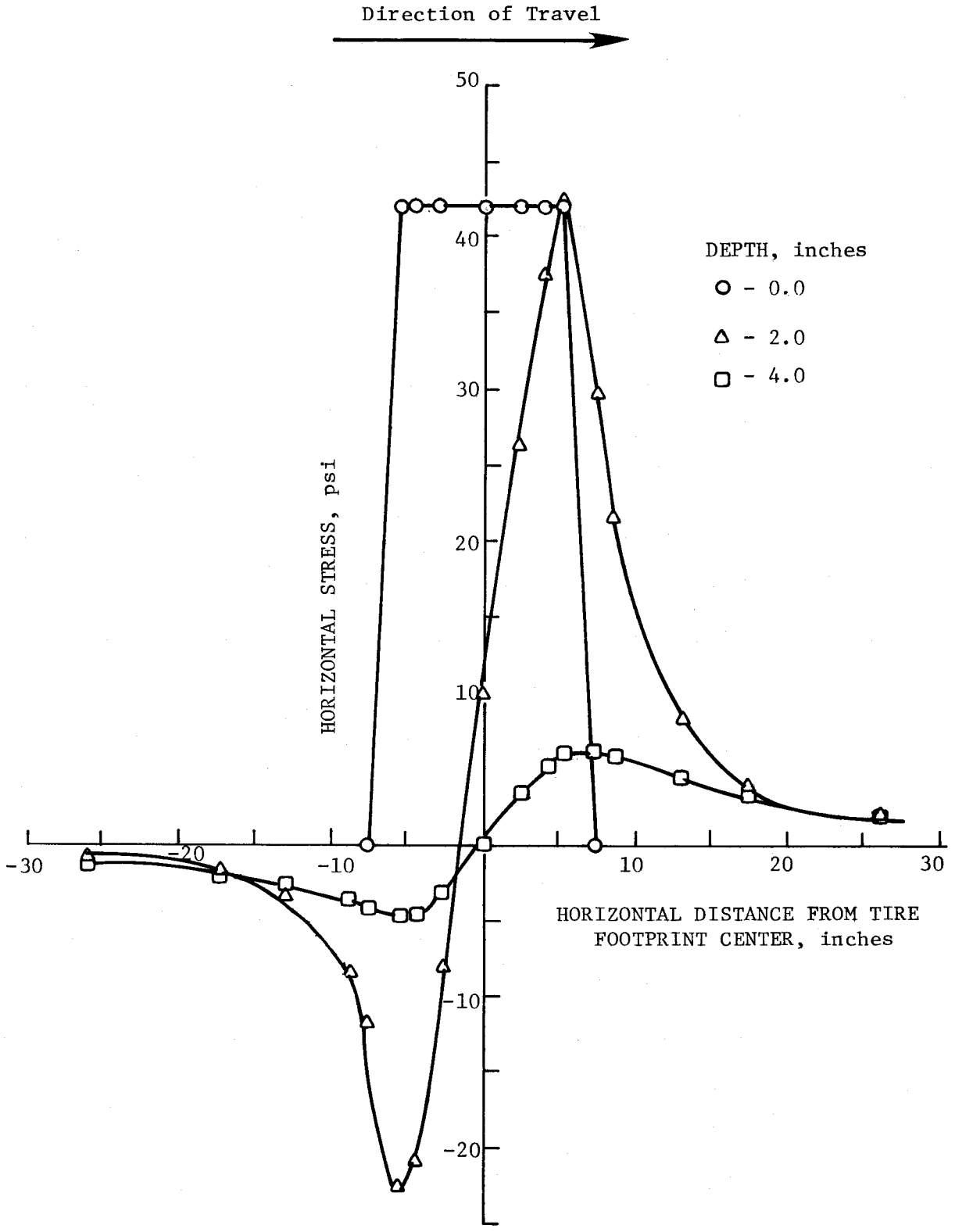

FIGURE B9. Horizontal Stress Distribution for Beechcraft King-Air on 2.0-inch Overlay

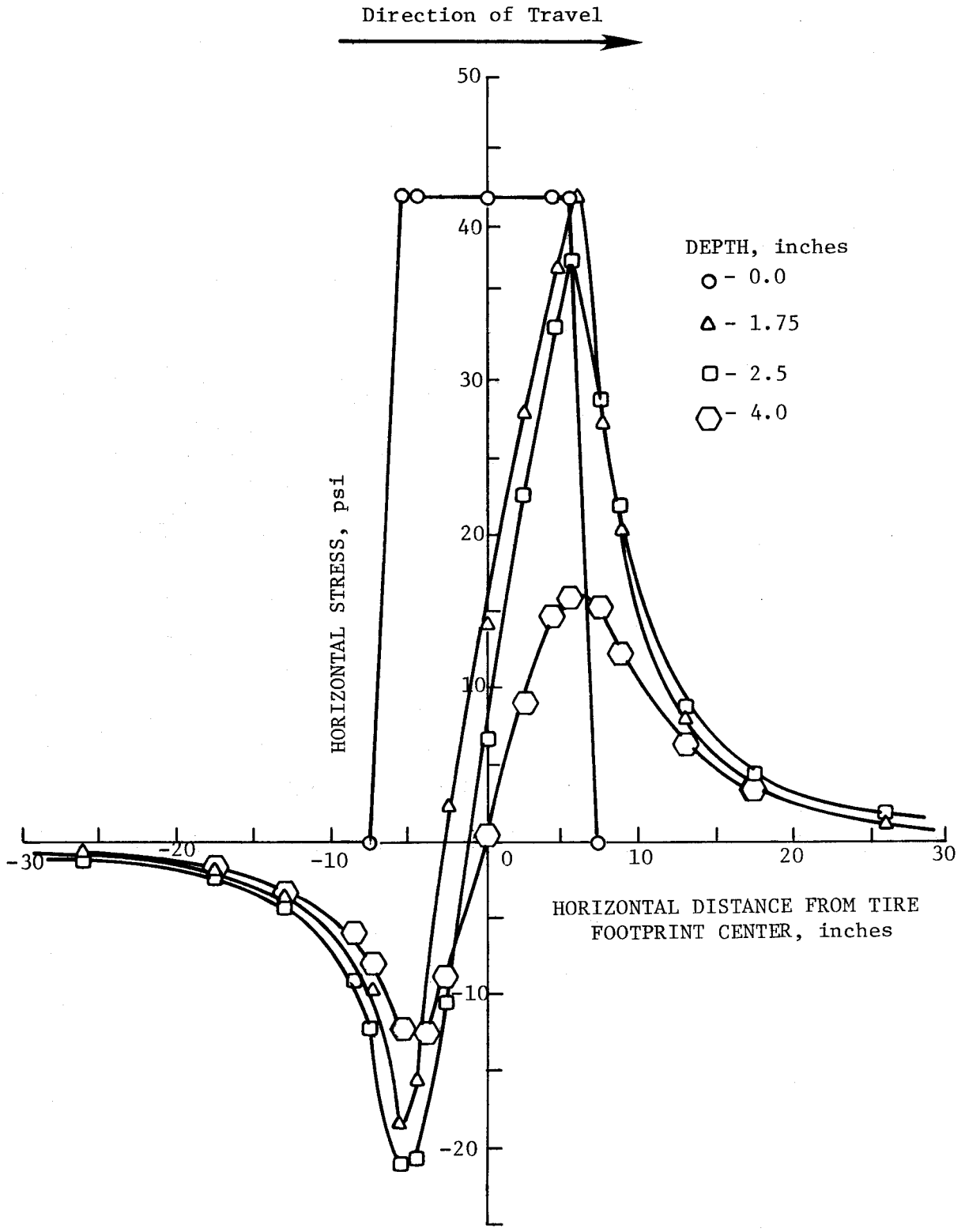

FIGURE B10. Horizontal Stress Distribution for Beechcraft King-Air on 2.5-inch Overlay

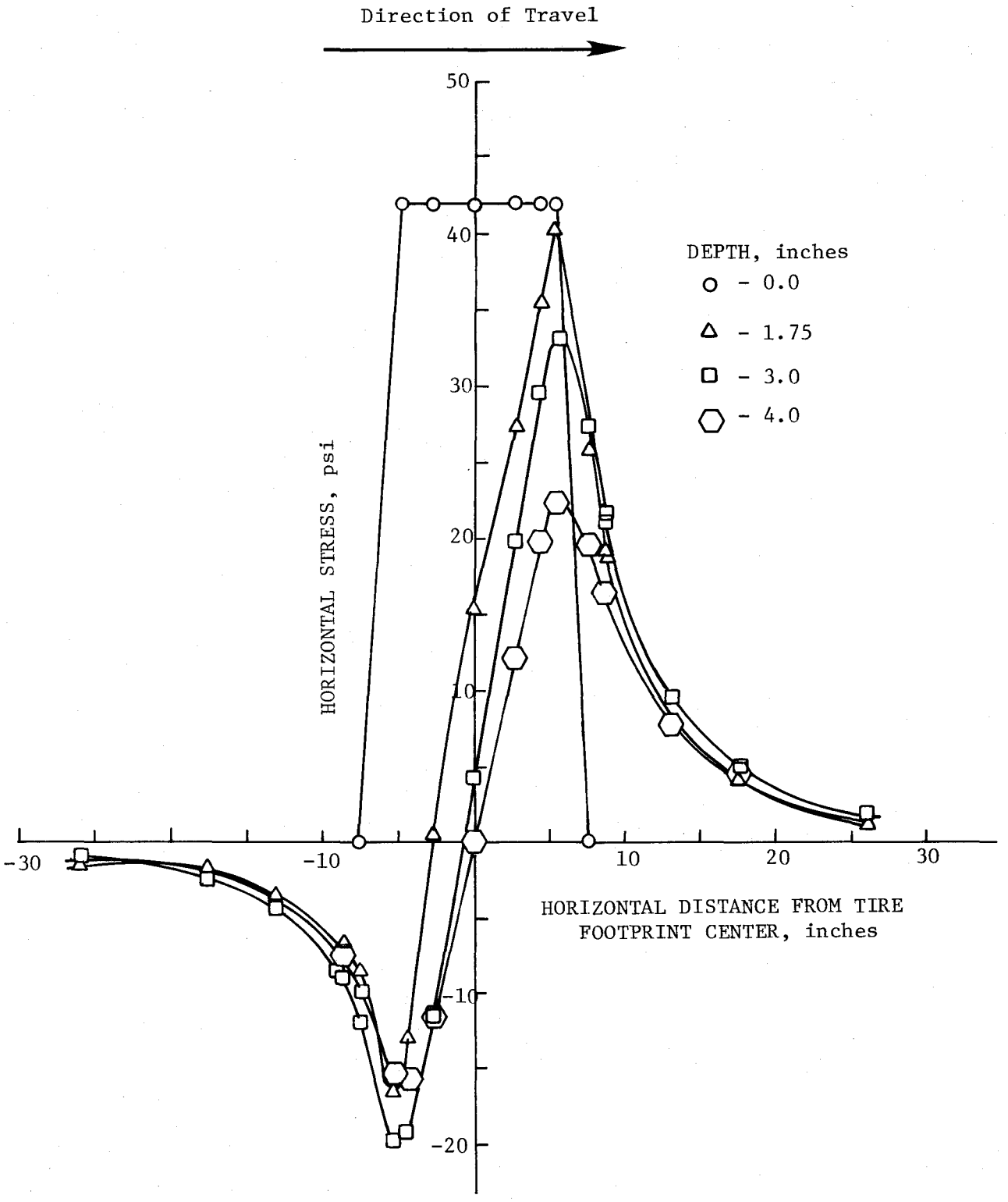

FIGURE B11. Horizontal Stress Distribution for Beechcraft King-Air on 3.0-inch Overlay

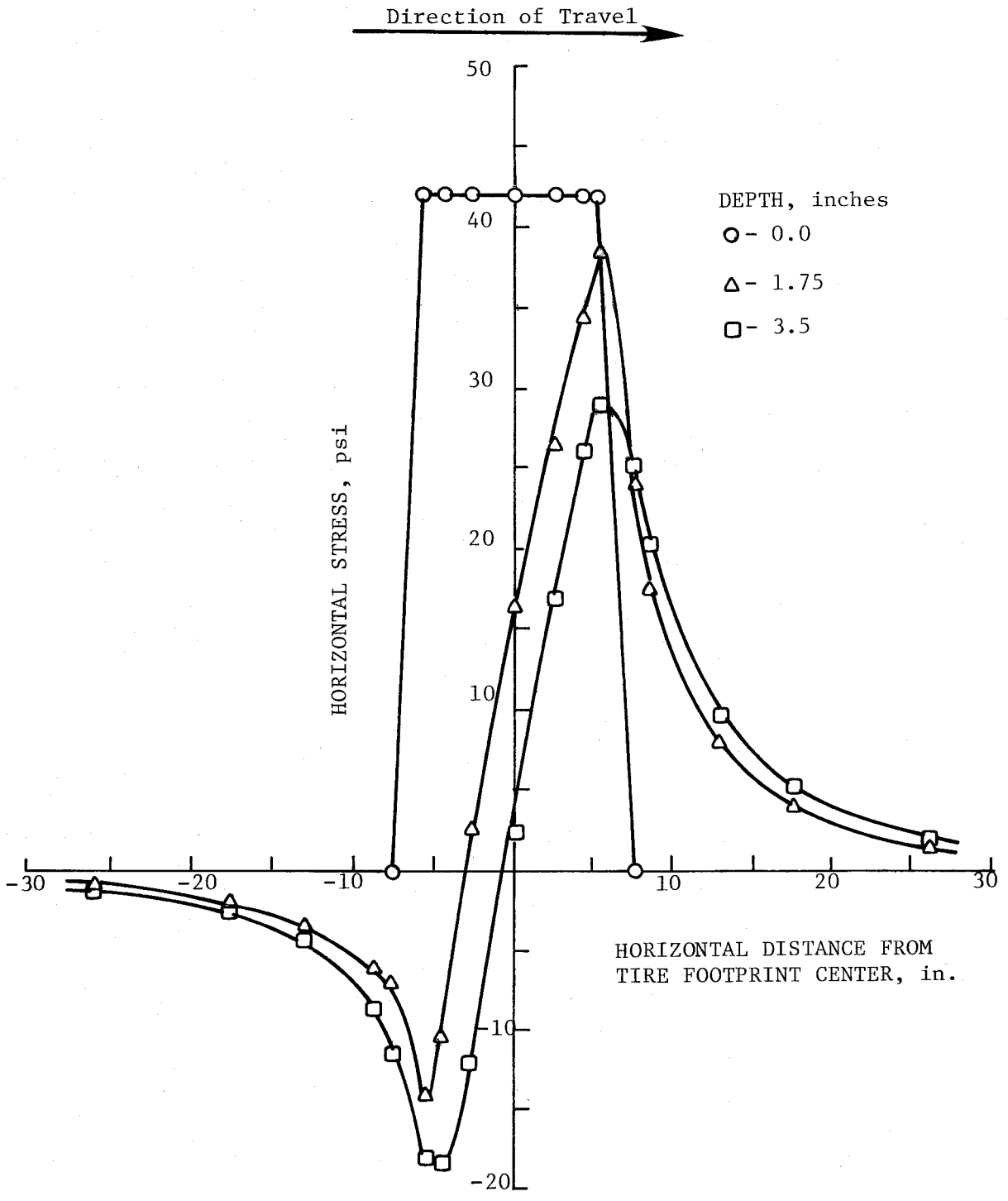

FIGURE B12. Horizontal Stress Distribution for Beechcraft King-Air on 3.5-inch Overlay

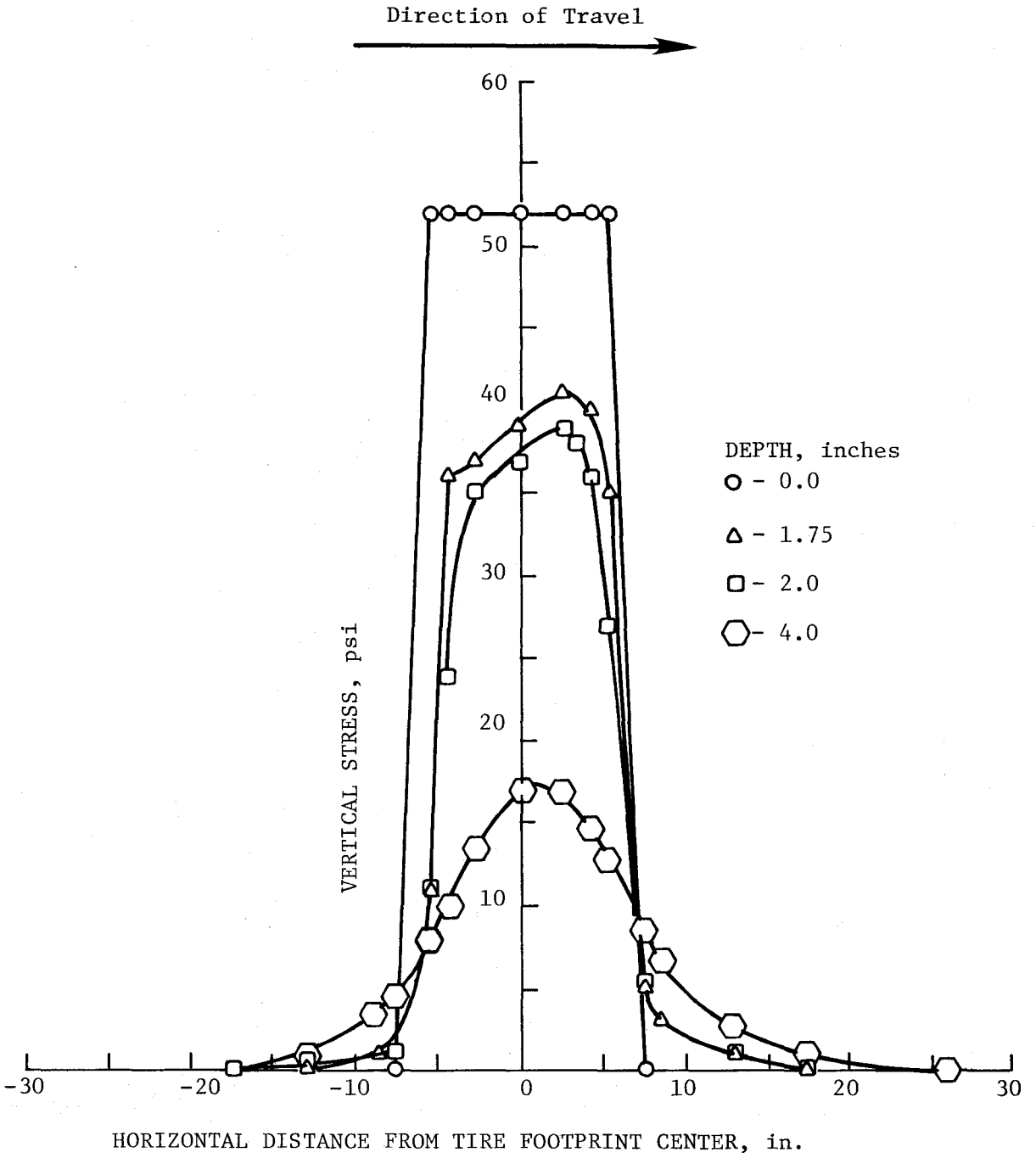

FIGURE B 13. Vertical Stress Distribution for Beechcraft King-Air on 2.0-inch Overlay

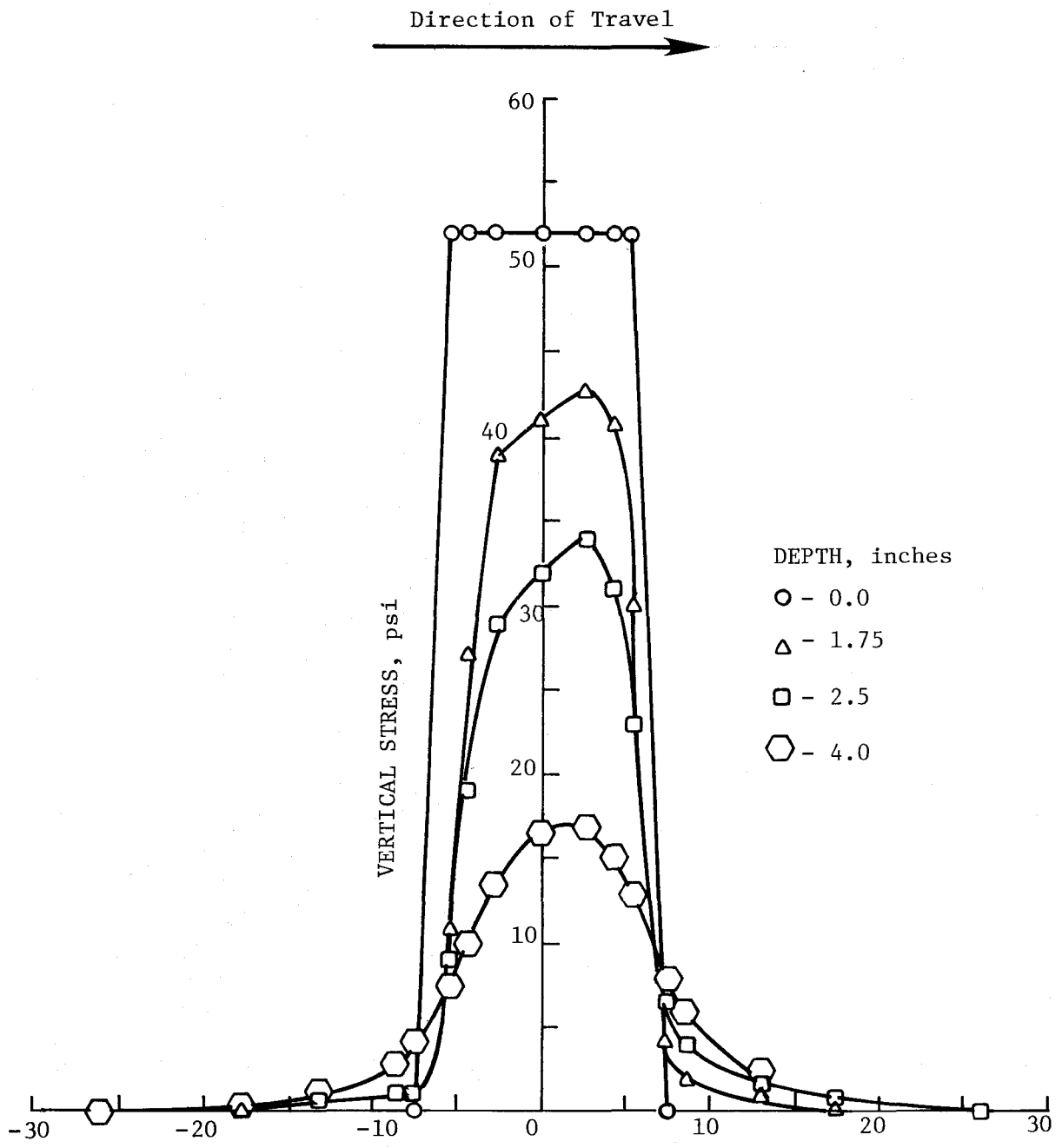

FIGURE B14. Vertical Stress Distribution for Beechcraft King-Air on 2.5-inch Overlay

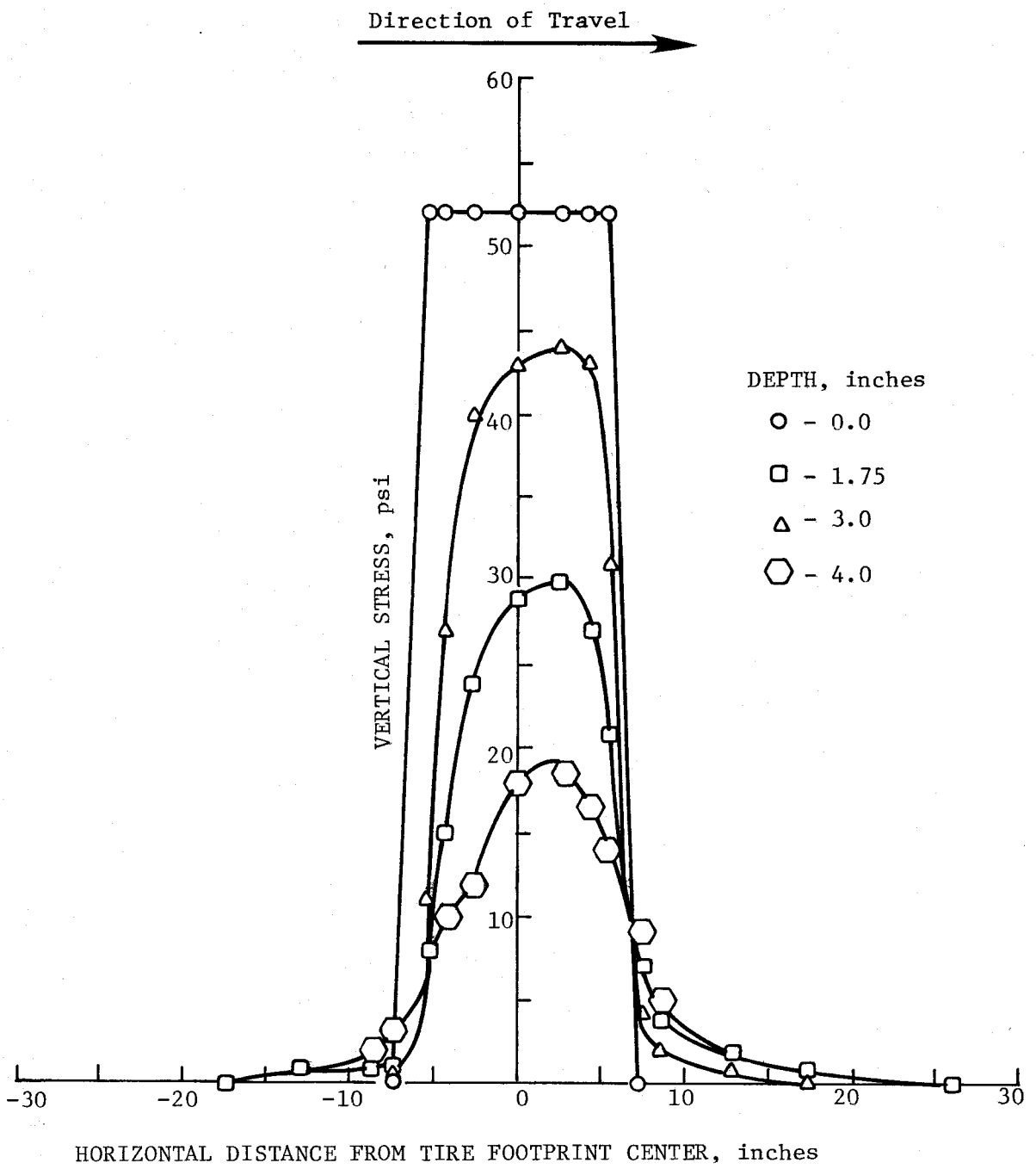

FIGURE B15. Vertical Stress Distribution for Beechcraft King-Air on 3.0-inch Overlay

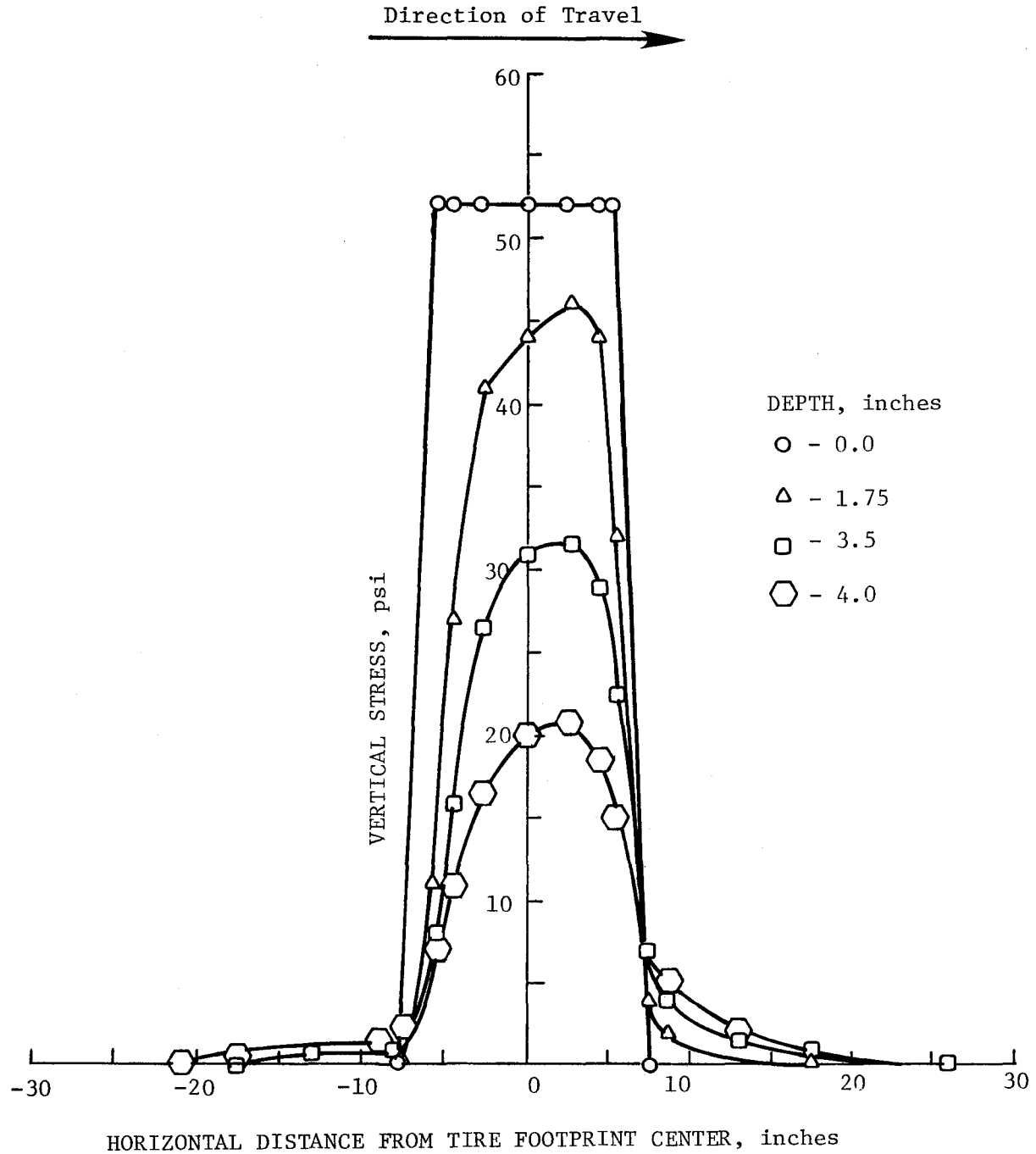

FIGURE B16. Vertical Stress Distribution for Beechcraft King-Air on on 3.5-inch Overlay